Steady-State and Dynamic Properties of Cardiac Sodium-Calcium Exchange

Ion and Voltage Dependencies of the Transport Cycle

SATOSHI MATSUOKA and DONALD W. HILGEMANN

From the Department of Physiology, University of Texas Southwestern Medical Center at Dallas, Dallas, Texas 75235

ABSTRACT Ion and voltage dependencies of sodium-calcium exchange current were studied in giant membrane patches from guinea pig ventricular cells after deregulation of the exchanger with chymotrypsin. (*a*) Under *zero-trans* conditions, the half-maximum concentration (K_h) of cytoplasmic calcium (Ca_i) for activation of the isolated inward exchange current decreased as the extracellular sodium (Na_o) concentration was decreased. The K_h of cytoplasmic sodium (Na_i) for activation of the isolated outward exchange current decreased as the extracellular calcium (Ca_o) concentration was decreased. (*b*) The current–voltage (*I-V*) relation of the outward exchange current with saturating concentrations of Na_i and Ca_o had a shallow slope (twofold change in ~100 mV) and a slight saturation tendency at very positive potentials. The outward current gained in steepness as the Na_i concentration was decreased, such that the K_h for Na_i decreased with depolarization. The decrease of K_h for Na_i with depolarization was well described by a Boltzmann equation ($e^{\alpha \cdot Em/26.6}$) with a slope (α) of −0.06. (*c*) Voltage dependence of the outward current was lost as the Ca_o concentration was decreased, and the K_h for Ca_o increased upon depolarization with a Boltzmann slope of 0.26. (*d*) The *I-V* relation of the inward exchange current, under *zero-trans* conditions, was also almost linear (twofold change in ~100 mV) and showed some saturation tendency with hyperpolarization as the Ca_i concentration was decreased. The K_h for Ca_i decreased with depolarization (Boltzmann slope, −0.10). Voltage dependence of the inward current was decreased in the presence of a high (300 mM) Na_o concentration. (*e*) In the presence of both Na and Ca on both membrane sides, the *I-V* relations with saturating Na_i show sigmoidal shape and clear saturation at positive potentials. Measured reversal potentials were close to the equilibrium potential expected for a 3 Na to 1 Ca exchange. (*f*) Na_i and Ca_i interacted competitively with respect to the outward current, but in a mixed competitive–noncompetitive fashion with respect to the inward current. (*g*) Ca_i inhibited the outward exchange current in a voltage-dependent manner. The half-effective concentration for inhibition (K_i) by Ca_i increased upon depolarization with a Boltzmann slope of 0.32 in 25 mM Na_i and

Address reprint requests to Donald W. Hilgemann, Department of Physiology, University of Texas Southwestern Medical Center at Dallas, 5323 Harry Hines Blvd., Dallas, TX 75235.

J. GEN. PHYSIOL. © The Rockefeller University Press · 0022-1295/92/12/0963/39 $2.00 963
Volume 100 December 1992 963–1001

0.20 in 100 mM Na_i. (*h*) Na_i also inhibited the inward exchange current voltage dependently. The K_i decreased upon depolarization (Boltzmann slope, −0.11 at 3 μM Ca_i and −0.10 at 1.08 mM Ca_i). (*i*) All described exchange current characteristics were well explained by consecutive-type exchange models, assuming (*1*) multiple voltage- and time-dependent Na occlusion/deocclusion steps in the Na translocation pathway, (*2*) a small voltage dependence of Ca occlusion/deocclusion on the cytoplasmic side, and (*3*) the existence of a binding site configuration that can be occupied by 1 Na ion and 1 Ca ion on the cytoplasmic side.

INTRODUCTION

Electrophysiological studies of cardiac sodium-calcium exchange have progressed rapidly from the inferred existence of significant exchange current components (Horackova and Vassort, 1979; Mullins, 1979) to mechanism-oriented studies of exchange function (Li and Kimura, 1990, 1991; Gadsby, Noda, Shepherd, and Nakao, 1991; Hilgemann, Nicoll, and Philipson, 1991*b*), regulation (Collins, Somlyo, and Hilgemann, 1992; Hilgemann and Collins, 1992), and partial reactions (Niggli and Lederer, 1991; Hilgemann et al., 1991*b*). An understanding of the physical basis of electrogenicity has now become a realistic goal with the promise of important new insights into the exchange process. The search for clues about the electrogenic steps of sodium-calcium exchange was started with ion flux studies of self-exchange of both Na and Ca. If the exchange cycle is of the consecutive type, as recently suggested for the cardiac exchanger (Khananshvili, 1990; Li and Kimura, 1991; Hilgemann et al., 1991*b*), then the reaction pathways used for calcium-calcium exchange and sodium-sodium exchange will be made up of partial reactions of the normal exchange cycle. In squid axon, experiments of DiPolo and Beaugé (1990) revealed no voltage dependence of the sodium-sodium exchange mode and a monotonic decrease of calcium-calcium exchange with depolarization. For the reconstituted cardiac exchanger in proteoliposomes, no voltage dependence of either calcium-calcium or sodium-sodium exchange was found with saturating ion concentrations, and modest voltage dependence of both modes was found with low Ca and Na concentrations (Khananshvili, 1991). In barnacle muscle, no voltage dependence of sodium-sodium exchange has been revealed with saturating Na ion concentrations (Razgado-Flores, H., personal communication).

Recently, current transients interpreted as partial electrogenic reactions of the exchange cycle have been reported (Hilgemann et al., 1991*b*; Niggli and Lederer, 1991). Niggli and Lederer (1991) suggest that an inward current transient obtained during flash photolysis of caged calcium in myocytes reflects movement of negative charge through the membrane field during outward Ca translocation by the exchanger. Hilgemann et al. (1990*b*) suggest that outward current transients obtained during rapid cytoplasmic application of Na in giant excised patches with native or cloned cardiac exchanger reflect movement of positive charge through the membrane field during outward Na translocation. These authors concluded that most, if not all, voltage dependence of the exchange cycle lies in the Na translocation pathway. This conclusion was based first on their failure to identify current transients that could be associated with Ca translocation. Second, the conclusion was based on

effects of membrane voltage on the apparent ion affinities of exchange and effects of ion concentration changes on the *I-V* relations of exchange current.

The major goal of this study has been to extend and refine studies of the stationary exchange current in the context of specific transport models. For two reasons, we have chosen to begin detailed analysis of sodium-calcium exchange current with the chymotrypsin-deregulated exchanger. First, the cardiac sodium-calcium exchanger is strongly modulated by secondary processes that are themselves dependent on Ca_i and Na_i concentrations (Hilgemann, 1990; Hilgemann, Collins, and Matsuoka, 1992*a*; Hilgemann, Matsuoka, Nagel, and Collins, 1992*b*). These processes may have complicated previous studies of the exchange mechanism itself. Second, in our experience the modulation processes are remarkably variable between cell batches and/or animal batches. Chymotrypsin treatment not only greatly simplifies exchange function by functionally destroying secondary regulation, but exchanger function after chymotrypsin treatment is much less variable.

We demonstrate here (*a*) changes of apparent ion affinities with changes of counter-transported ion concentrations, (*b*) shape changes of the *I-V* relations for outward sodium-calcium exchange current with changes of both Na_i and Ca_o concentrations, (*c*) shape changes of the *I-V* relations for inward sodium-calcium exchange current with changes of both Na_o and Ca_i concentrations, (*d*) shape changes of both outward and inward exchange current *I-V* relations with inhibition by the counter-transported ion from the cytoplasmic side, and (*e*) competitive and noncompetitive interactions of Na and Ca on the cytoplasmic side. Finally, we demonstrate the minimum requirements of consecutive exchange models to account for all observed exchange current characteristics: (*a*) multiple voltage- and time-dependent occlusion/deocclusion steps in the Na pathway, (*b*) a small voltage dependence of Ca occlusion/deocclusion from the cytoplasmic side, and (*c*) the existence of a binding site conformation that can bind one Ca and one Na ion from the cytoplasmic side.

MATERIALS AND METHODS

Essentially the same methods described in a previous article (Hilgemann et al., 1992*b*) were used in this article.

In all experiments presented here, the cytoplasmic face of patch membranes was pretreated with 1–2 mg/ml chymotrypsin (Sigma Chemical Co., St. Louis, MO) until the exchange current was maximally activated (30–80 s). As reported in an accompanying article (Hilgemann et al., 1992*b*), voltage dependence of the fully activated outward sodium-calcium exchange current was not modified by chymotrypsin, and our experience with chymotrypsin treatment for the fully activated inward current was similar. Other conditions have not been tested.

Model Fitting Procedures

A least-squares method was used to fit experimental data to exchange models. This method used the generalized Newton method for simultaneous nonlinear equations given by Greenspan (1974). Parameters were improved in a randomized order in the course of each fitting cycle. In addition to the model-specific parameters, one scaler variable was fitted for each experiment. Individual experiments were weighted so that deviations of the modeled exchange function from experimental results were roughly equal for the various types of experiments

included in the data base. For the E4 and E8 models presented, data weighting resulted in little or no subjective improvement of the model fits. Results from 27 experiments were included for the data base fits presented in this article. Programs were written in Turbo Pascal (Borland International, Scotts Valley, CA) and were run on IBM-compatible personal computers.

RESULTS

Extracellular Cation Dependence of Outward Current

It has been reported that extracellular monovalent cations enhance calcium-calcium exchange and the calcium influx mode of sodium-calcium exchange in squid axon (Allen and Baker, 1986*a*, *b*; DiPolo and Beaugé, 1990) and the outward exchange current in cardiac myocytes (Gadsby et al., 1991). We therefore tested first for an effect of extracellular monovalent cations on the outward exchange current. Fig. 1 shows the *I-V* relations of the outward exchange current in the absence of external

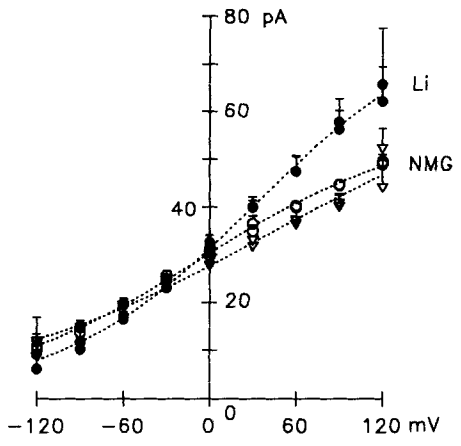

FIGURE 1. The effect of external monovalent cation on the *I-V* relations of the outward exchange current. Ca_o concentration is 5 mM. The outward current was activated by 100 mM Na_i. *I-V* relations of the outward current were first obtained without external monovalent cation (replaced with 140 mM NMG, *open circles*), then with 140 mM Li^+ (*filled circles*), and again without monovalent cation (*triangles*). Pipette solution was changed with the pipette perfusion method. Data are shown as mean, and error bars indicate the positive (+) SD (n = 4–6).

monovalent cation (replaced with 140 mM NMG) and in the presence of 140 mM external Li^+. The Ca_o concentration is 5 mM. The pipette solution was changed via the pipette perfusion device from 140 mM NMG solution (open circles) to 140 mM Li^+ solution, and then again to the initial 140 mM NMG solution. The outward exchange current was activated by application of 100 mM Na_i. The *I-V* relations increased somewhat in steepness and lost their tendency to saturate with 140 Li^+, and the effects were reversible. Gadsby et al. (1991) described the outward exchange current in the presence of 145 mM Li^+ and found an almost complete loss of voltage dependence in the absence of Li^+ (replaced with NMG). The Li^+ effect that we demonstrate is small compared with their results. It was also small when Ca_o concentrations were nonsaturating for the outward current. It is noted that under our experimental conditions, external Li^+ usually somewhat increases the background patch conductance (i.e., leak current) and tends to destabilize patches.

Description of Exchange Models Fitted to Data Base

Three related models of the sodium-calcium exchange cycle are presented in Fig. 2. As shown subsequently, these models illustrate the minimum common assumptions needed to fit the experimental data on the basis of our experience to date. Therefore, these three models should be useful in future work. The mathematical

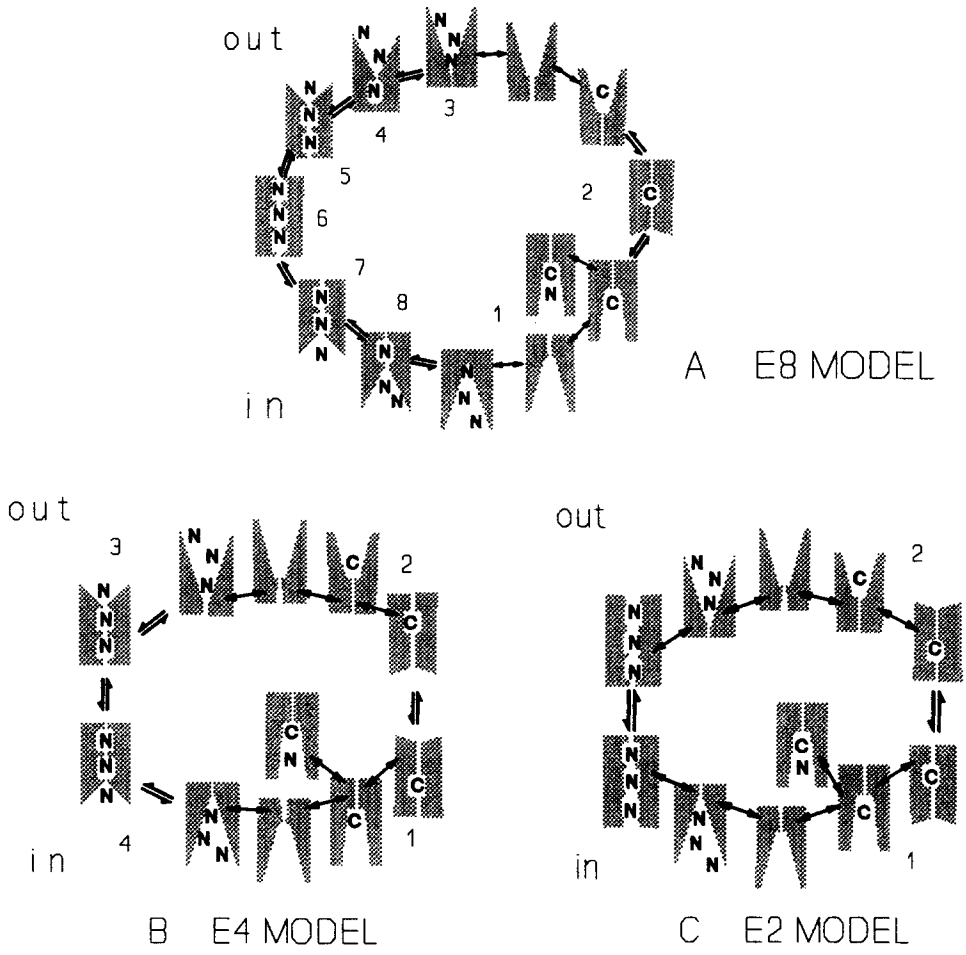

FIGURE 2. State diagrams of three consecutive sodium-calcium exchange models. (*A*) E8 model; (*B*) E4 model; (*C*) E2 model. See text for details.

formulation of the models is presented in the Appendix. In each model it is assumed that ion binding is instantaneous and voltage independent. All three Na ions can bind and unbind from the empty carrier. Electrogenicity occurs exclusively with occlusion of ions into the transporter protein. This process is conceptualized as the "tightening" of a pore or closing of a zipper (Tanford, 1982), presumably associated with dehydration of the pore, and thereby the partial movement of electrical field

across both the bound ions and ion binding sites. Double-bar arrows in each panel of Fig. 2 correspond to kinetic transitions between states, and single, two-headed arrows indicate reactions treated as instantaneous equilibria within each state. E1 in each model corresponds to a state with all binding sites available from the cytoplasmic side. To allow fitting, it must be assumed that one Na ion can bind to the Ca-occupied exchanger in this state. Na binding is assumed to be sequential. For simplicity, the affinities of the second and third Na binding sites are assumed not to change as the first (and second) Na ions are occluded. Microscopic reversibility is enforced in all simulations, and total charge movement per cycle is one charge through the entire membrane electrical field. Perfect 3 Na to 1 Ca stoichiometry is given in all simulations.

The three models will be referred to as the E8, E4, and E2 models, corresponding to the assumption of 8, 4, and 2 kinetically defined states, respectively. For the E8 model, occlusion of each ion is simulated. Within the E_1 and E_3 states, three Na ions can bind and dissociate freely, within the E_8 and E_4 states two Na ions can bind and dissociate, and within the E_7 and E_5 states only one Na ion can bind and dissociate. For simplicity, all rate constants are equal in fits presented, the charge movements occurring in the six Na occlusion reactions are also equal, and the cytoplasmic Na ion that binds to the Ca-loaded configuration does so with the same affinity as the third Na ion. With these constraints, the parameters that must be fitted are the ion affinities (four for the cytoplasmic side and four for the extracellular side) and the fractional charge movements occurring during two of the occlusion reactions.

For the E4 model simulations presented, Na translocation is simplified such that all charge movement occurs with the occlusion of the first two ions bound on each side (E_2-E_3 and E_1-E_4 transitions). This specific assumption allows reproduction of nearly all results simulated with the E8 model. Occlusion of the third Na ion and deocclusion of the first Na ion occurs simultaneously without electrogenicity (E_3-E_4 transition). Occlusion and deocclusion of Ca are treated as instantaneous reactions in this model, and equivalent to the E_3-E_4 transition, these reactions are separated by a time-dependent, voltage-independent transition (E_1-E_2). For simplicity, the time-dependent reactions are assigned the same rate constant, the magnitudes of charge movement during occlusion of Na on the cytoplasmic and extracellular sides are equal, and occlusion of extracellular Ca is assumed to be electroneutral. Thus, only the magnitude of one of the charge movements and the ion affinities must be fitted.

For the E2 model, ion occlusion takes place instantly on either side when binding sites are occupied by either three Na ions or one Ca ion. These reactions are separated by time-dependent, voltage-independent reactions (E_1-E_2 transitions). For the best fit with the E2 model, given in the Appendix, the occlusion and deocclusion of Ca from the extracellular side are assumed to be electroneutral.

One set of parameters for each model, as used in this article, is given in the Appendix. The E2 model is the simplest model that reproduces most results well, the major exception being *I-V* relations with reduced ion concentrations. The E4 model is the simplest model tested that describes all experimental results well. It is noted that this success depends on the placement of charge movement between sodium binding reactions on each side (i.e., after the second sodium ion binding reaction). The E8 model, with individual treatment of each sodium occlusion reaction, in our

opinion represents the minimum complexities of the actual exchange cycle. All simulations presented use the minimum number of parameters, which, in our experience, allows accurate reproduction of the data base on stationary exchange current.

Zero-trans Ion Dependencies at 0 mV

Fig. 3 presents ion dependencies of the exchange current at a membrane potential of 0 mV under *zero-trans* conditions (i.e., with only one transported ion species on each side). Solid curves are the fit to the E4 model. Fig. 3, *A*, *C*, and *D* are results from experiments using the pipette perfusion method.

Fig. 3 *A* shows the Ca_i dependence of the inward exchange current at three different Na_o concentrations: 50 mM (filled circles), 80 mM (triangles), and 150 mM (open circles), respectively. As described previously (Hilgemann et al., 1991*b*; Hilgemann, Collins, Cash, and Nagel, 1991*a*), the half-maximal concentration (K_d) for Ca_i decreases with reduction of Na_o. Here, the model-based K_d decreases from 6.9 μM to 2.7 and 0.84 μM when Na_o is reduced from 150 mM to 80 and 50 mM, respectively.

Fig. 3 *B* shows the Na_o concentration dependence of the inward exchange current. This result, and only this result, is from an outside-out patch. Outside-out patches could be obtained routinely in individual myocyte batches during attempts to disrupt vesicles upon patch excision (Collins et al., 1992). Solutions are the usual outward current solutions. Accordingly, the cytoplasmic surface (i.e., on the pipette side; not chymotrypsin treated) is exposed to 5 mM Ca. To obtain the complete Na dependence of the current, hypertonic solutions were used, substituting Na-MES for a mixture of equal parts of Li-MES and Cs-MES. As apparent from the data fits, Na_o dependence of the current in the outside-out patch is consistent with that obtained in pipette perfusion experiments with the deregulated current (Fig. 3 *A*), whereby more data points are readily obtained with the outside-out patches. The K_d for Na_o was 118 mM.

Fig. 3 *C* shows the Na_i dependence of outward exchange current at 2.0 and 0.35 mM Ca_o. As described previously (Hilgemann et al., 1991*a*, *b*), the K_d for Na_i decreases as the Ca_o concentration is decreased, here from 18.6 to 13.2 mM. Note here that the multi-step consecutive models, in agreement with the experimental data, do not predict a simple relationship between the maximum current and the K_d for Na_i. In these results, the modeled maximum current decreases by 45% and the modeled K_d decreases by 24%. Fig. 3 *D* shows the Ca_o dependence of the outward current. The modeled K_d was 0.32 mM.

Asymmetry of the ion dependencies of sodium-calcium exchange are well described in squid axon (DiPolo and Beaugé, 1990) and cardiac myocytes (Miura and Kimura, 1989). Apart from demonstrating data fits of the *zero-trans* ion dependencies, this data set demonstrates the degree of asymmetry of the exchange system in giant patch experiments. For the maximally activated inward and outward currents, the half-maximal Na concentrations are approximately eightfold greater on the extracellular side, while the half-maximal Ca concentrations are ~100-fold greater on the extracellular side. Finally, it is mentioned that nearly maximal inward and outward exchange currents were determined in a patch at 0 mV using the pipette perfusion

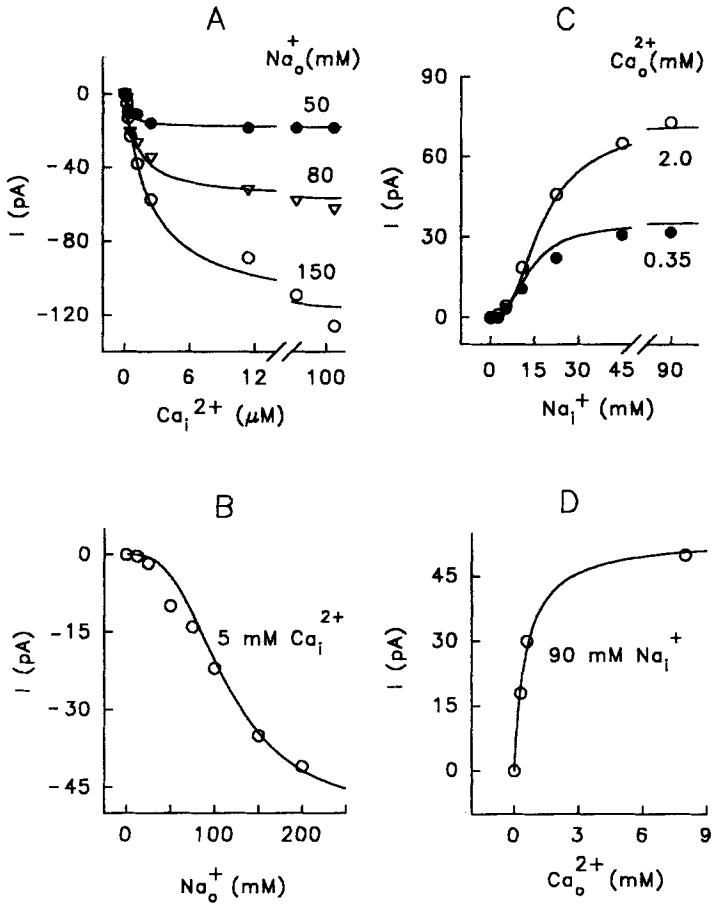

FIGURE 3. Ion concentration dependences of the exchange current at a membrane potential of 0 mV under *zero-trans* conditions. (*A*) Cytoplasmic Ca (Ca_i) dependence of the inward exchange current at three different extracellular Na (Na_o) concentrations in a patch. Na_o concentrations are 50 mM (*filled circles*), 80 mM (*triangles*), and 150 mM (*open circles*). The K_d values from model fits of the data for Ca_i are 0.84, 2.7, and 6.9 μM, respectively. (*B*) Na_o dependence of the inward exchange current from an outside-out patch. Ca_i (in pipette) concentration is 5 mM. K_d for Na_o is 118 mM. (*C*) Cytoplasmic Na (Na_i) dependence of the outward exchange current at extracellular Ca (Ca_o) concentrations of 2.0 (*open circles*) and 0.35 mM (*filled circles*). The K_d values from model fits of the data for Na_i are 18.6 and 13.2 mM, respectively. (*D*) Ca_o dependence of the outward exchange current. Na_i concentration is 90 mM. The K_d value from model fits of the data is 0.32 mM.

method. The outward current (5 mM Ca_o/100 mM Na_i) was 25% greater than the inward current (150 mM Na_o/100 μM Ca_i).

The Outward Exchange Current I-V: Sodium Dependence

Fig. 4 shows *I-V* relations from −125 to +100 mV of the outward exchange current at Na_i concentrations of 6, 12, 25, 50, and 100 mM with 8 mM Ca_o, typical for three

similar experiments in this series. At saturating Na_i concentrations, the *I-V* relation is almost linear, except at very negative potentials. The *I-V* relation has a slight saturation tendency at very positive potentials. The current just doubles in 100 mV. In Fig. 4 *B*, the currents are normalized to the peak value at +100 mV. The current gains in steepness as the Na_i concentration is reduced. At 6 mM Na_i, the current doubles in just 52 mV and takes on a more exponential shape.

Fig. 5 *A* presents these data in the concentration format, whereby the Na_i concentration dependence of the current has been fitted at different potentials to a Hill equation (dotted lines). The half-maximal concentration (K_h) values and Hill coefficient (n_h) values are presented in Fig. 5 *B*. The K_h decreases upon depolariza-

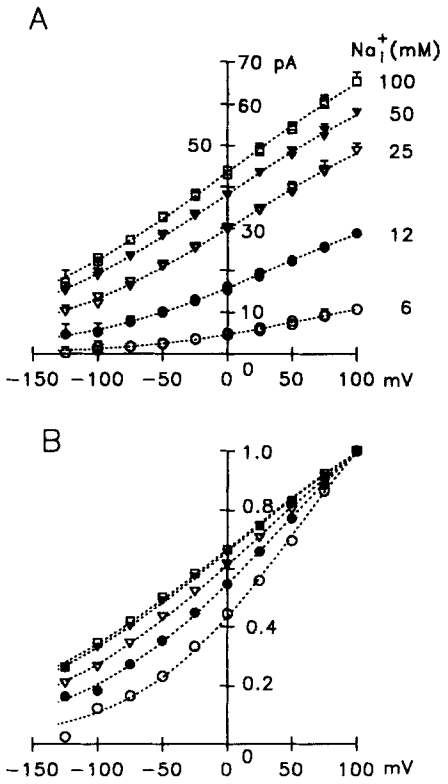

FIGURE 4. Na_i dependence of the outward exchange *I-V* relation. (*A*) *I-V* relations of the outward exchange current at different Na_i concentrations. Na_i concentrations (millimolar) are shown at the right side of each *I-V* relation. Data show mean + SD. (*B*) Normalized *I-V* relations of the outward current at different Na_i concentrations. Data from *A* are normalized by an average amplitude at 100 mV and mean values are shown. Same symbols as in *A*.

tion from a value of 23.1 mM at −100 mV to a value of 14.5 mM at +100 mV. Hill coefficients are close to 2 and remain unchanged with changes of potential. A decrease in the K_h value at −125 mV was not observed in other patches. The best fit of the K_h values to a Boltzmann equation had a slope of −0.06. This voltage-dependent change of the K_h for Na_i is consistent with the idea of a small high resistance access channel or "ion well" (Läuger, 1987, 1991). However, consecutive models without any ion well properties, as used in this article, display these behaviors equally and accurately describe these results (Fig. 11).

It is noted that in a previous series of experiments with observations on patches from both guinea pig and rabbit myocytes (>15 observations; Hilgemann et al., 1991*b*) significant shifts of the K_h value were not obtained with changes of membrane potential, whereby potential was stepped continuously at 1-s intervals between −80 and +20 mV. We do not know the reason for the difference at this time.

The Outward Exchange Current I-V: Calcium Dependence

Fig. 6 shows the outward exchange current at different Ca_o concentrations. Fig. 6 *A* shows the pipette perfusion protocol used, activating the current in all cases by

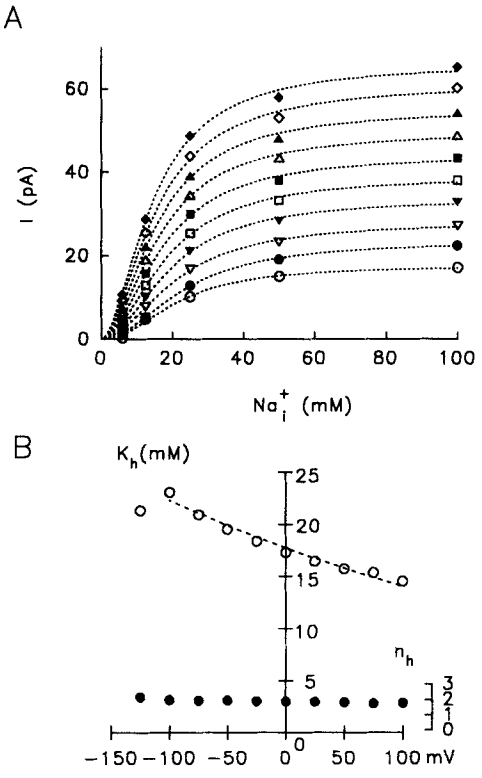

FIGURE 5. Na_i dependence of the outward current at different membrane potentials. Data from Fig. 4. Values of current amplitude are plotted against Na_i concentration. Membrane potentials are 100 mV (*filled diamonds*), 75 mV (*open diamonds*), 50 mV (*filled triangles*), 25 mV (*open triangles*), 0 mV (*filled squares*), −25 mV (*open squares*), −50 mV (*filled inverted triangles*), −75 mV (*open inverted triangles*), −100 mV (*filled circles*), and −125 mV (*open circles*). Dotted lines are fitted Hill equations. (*B*) Membrane potential dependence of K_h and n_h. K_h (*open circles*) and n_h (*filled circles*) values for fitting the Hill equation are plotted against membrane potentials. A scale for n_h is shown at the right side of the figure. A dotted line is a fitted Boltzmann equation, $K_h = 17.7 \cdot e^{-0.06 \cdot Em/26.6}$.

cytoplasmic application of 100 mM Na_i. *I-V* relations were obtained first at 0.2 mM Ca_o, then after changing pipette solutions to 10 mM Ca_o, followed by incremental reduction to 1.2, 0.8, 0.4, and again 0.2 mM Ca_o. Note the stability of current under these conditions.

I-V relations for the outward current are plotted in Fig. 6 *B*. With 10 mM Ca_o the *I-V* relation is as just described, doubling in just 100 mV. With reduction of the Ca_o concentration to 1.2, 0.8, and 0.4 mM, the current at positive potentials decreases markedly while the current at −120 mV hardly decreases at all. At 0.4 mM the current is nearly voltage independent, and with reduction of Ca_o to 0.2 mM the current decreases at all potentials. A clear negative slope of the outward exchange

current was never obtained at low Ca_o concentrations in this experimental series. Small negative slopes have been obtained with rabbit myocyte membrane. The almost complete loss of voltage dependence with 0.2 mM Ca_o was an invariable experimental result.

Amplitudes of the current at different membrane potentials were plotted and fitted to Hill equations (not shown). Fig. 6 *C* shows the fitted K_h (open circles) and n_h (filled circles) values. The K_h for Ca_o increases from 0.18 mM at −120 mM to 0.79 mM at +60 mV. At 0 mV the K_h is 0.44 mM. The slope of the fitted Boltzmann equation for

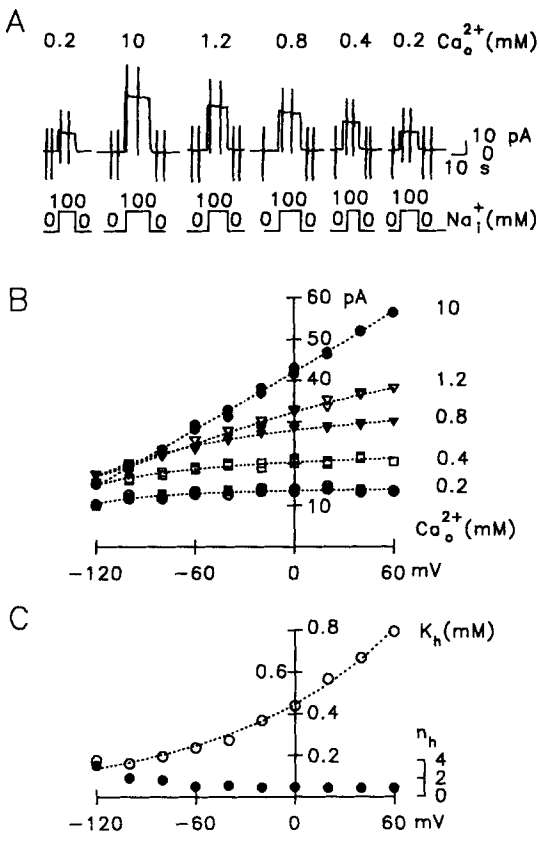

FIGURE 6. Ca_o dependence of the outward *I-V* relation. (*A*) Representative current records at 0 mV with different Ca_o concentrations in a patch. Ca_i concentration is 1 μM. Ca_o concentrations are shown above the corresponding current trace. The outward currents were activated by 100 mM Na_i. Voltage pulses were applied at spikes of the record. (*B*) *I-V* relations of the outward exchange current at different Ca_o concentrations. Ca_o concentrations are shown at the right of each *I-V* relation. Note that *I-V* relations at the first 0.2 mM (*open circles*) and the last 0.2 mM (*filled circles*) of Ca_o are identical. (*C*) Voltage dependence of K_h and n_h. K_h (*open circles*) and n_h (*filled circles*) values for fitting the Hill equation are plotted against membrane potential. A scale for n_h is shown at the right side of the figure. The dotted line is a fitted Boltzmann equation, $K_h = 0.45 \cdot e^{0.26 \cdot Em/26.6}$.

these results was 0.26 (dotted line). As shown in the lower part of the graph, the Hill coefficient appears to increase significantly from 1 to ~2.0 at −80 mV and 3.4 at −120 mV.

The Inward Exchange Current I-V: Calcium Dependence

Fig. 7 presents *I-V* relations of the *zero-trans* inward exchange current at different Ca_i concentrations with 150 mM Na_o. The *I-V* relations are remarkably linear with current decreasing by ~50% in 100 mV. In Fig. 7 *B* the *I-V* relations from *A* are normalized to the current values of each relationship at +60 mV. There is some

flattening of the relations at low Ca_i concentrations, but the slopes are different by only ~10%. Fig. 7 *C* shows the Hill parameters plotted against membrane potential. The K_h values decrease from 6.3 μM at −120 mV to 3.3 μM at +60 mV. The slope of the fitted Boltzmann equation is −0.10. The slope values of the Hill equations are very close to 1 and show no change.

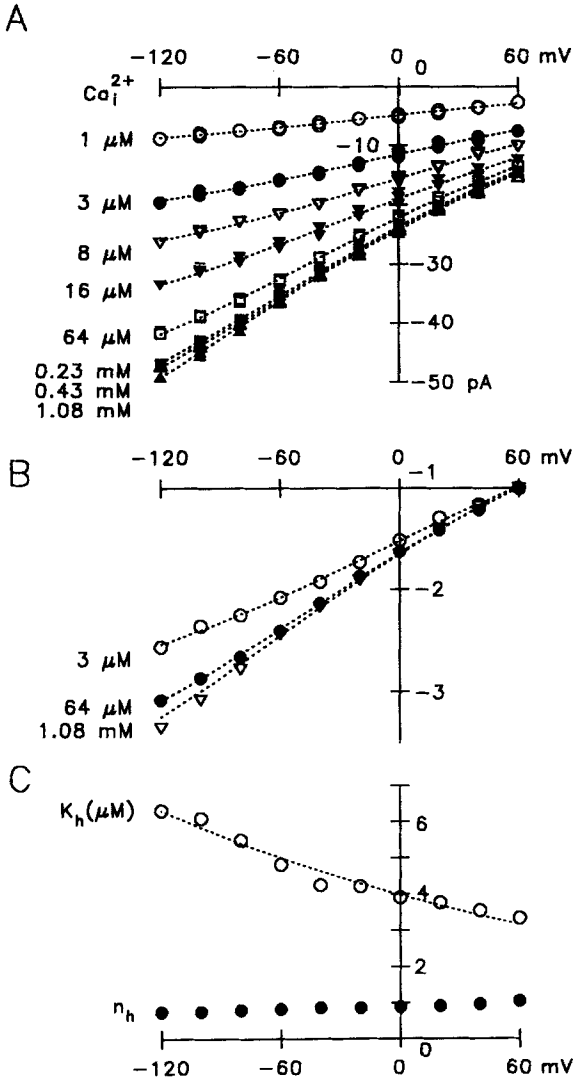

FIGURE 7. Ca_i dependence of the inward exchange *I-V* relation. (*A*) *I-V* relations of the inward exchange current at different Ca_i concentrations. 0 mM Ca_o, 150 mM Na_o, and 0 mM Na_i. Ca_i concentrations are 1 μM (*open circles*), 3 μM (*filled circles*), 8 μM (*open inverted triangles*), 16 μM (*filled inverted triangles*), 64 μM (*open squares*), 0.23 μM (*filled squares*), 0.43 μM (*open triangles*), and 1.08 mM (*filled triangles*). (*B*) Normalized *I-V* relations; data from *A*. Ca_i concentrations are 3 μM (*open circles*), 64 μM (*filled circles*), and 1.08 mM (*triangles*). (*C*) Membrane potential dependencies of fitted K_h and n_h. K_h (*open circles*) and n_h (*filled circles*) values for fitting the Hill equation are plotted against membrane potential. A fitted Boltzmann equation (*dotted line*) is $K_h = 4.0 \cdot e^{-0.10 \cdot Em/26.6}$.

Two differences from previous results (Hilgemann et al., 1991*b*) are noted. First, the slopes of *I-V* relations in this series of experiments are as much as 40% smaller than those found in a previous series of experiments including both rabbit and guinea pig myocytes. Second, the shifts of K_h values for a 100-mV change of membrane potential are smaller by ~50% than found previously.

The Inward Exchange Current I-V: Sodium Dependence

Fig. 8 shows *I-V* relations of the inward exchange current at 300 and 50 mM Na_o. Cs was substituted for Na in the pipette. Results at 300 mM Na_o are with 6 μM Ca_i (filled circles) and 1.4 mM Ca_i (filled triangles), and results at 50 mM Na_o are shown with 6 μM (open circles) and 1.4 mM Ca_i (open triangles). Note that with 50 mM Na_o the inward exchange current is completely saturated at 6 μM free Ca_i. This result is consistent with the results in Fig. 3. Fig. 8 *B* shows the *I-V* relations from *A* with 6 μM Ca_i, normalized to the current magnitudes at +60 mV. In the negative potential

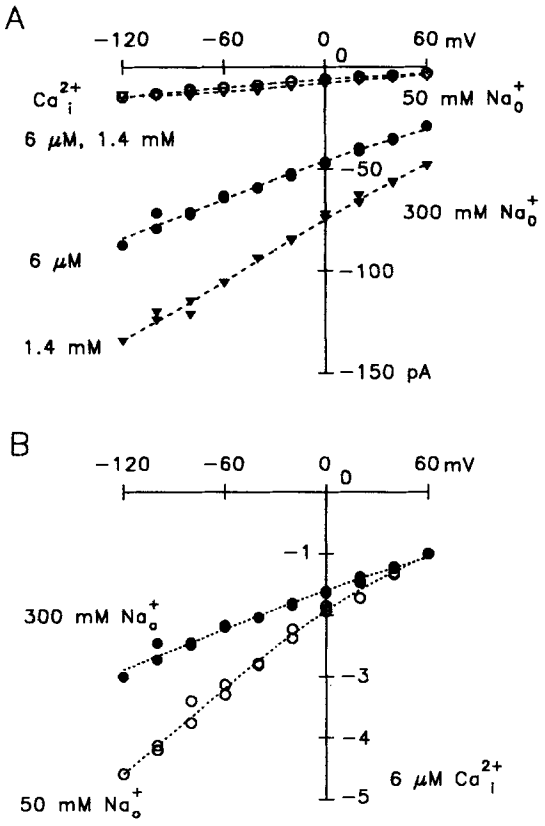

FIGURE 8. Na_o dependence of the inward exchange current. (*A*) *I-V* relations at 50 and 300 mM Na_o in a patch. Ca_i concentrations are 6 μM (*open circles*) and 1.4 mM (*open inverted triangles*) at 50 mM Na_o, and 6 μM (*filled circles*) and 1.4 mM (*filled inverted triangles*) at 300 mM Na_o. Ca_o and Na_i concentrations are 0 mM. (*B*) Normalized *I-V* relations. Ca_i concentration is 6 μM. *I-V* relations at 50 mM (*open circles*) and 300 mM (*filled circles*) Na_o in *A* are normalized by current amplitudes at 60 mV.

range, the slope of the *I-V* relation at 300 mM Na_o is decreased by ~47% in comparison to the relationship with 50 mM Na_o. The changes of slope are qualitatively similar to, but smaller in magnitude than those found in a previous series of experiments (Hilgemann et al., 1991*b*).

The Mixed Exchange Current I-V: Reversal Potential Measurements

I-V relations with both transported ions on both sides are of great interest. These conditions are the most physiologically relevant ones, and the reversals of these *I-V* relations are critical for an understanding of exchange stoichiometry. Fig. 9 presents

our best estimates of *I-V* relations with 2 mM Ca_o and 150 mM Na_o. The records in Fig. 9 *A* are with 1 μM Ca_i, and the records in Fig. 9 *B* are with 0.1 μM Ca_i. The results were obtained by subtracting membrane currents in the absence of Na_i and Ca_i from the respective membrane currents in their presence. We tested carefully to make sure that the Ca_i concentration changes resulted in no significant current shifts in experiments with no Na or Ca in the pipette (see Fig. 3 of Hilgemann et al., 1992*b*). Reversal potentials were determined by fitting the *I-V* relations to the smoothing equation used to generate figure curves and calculating the reversal potential from the fitted equation.

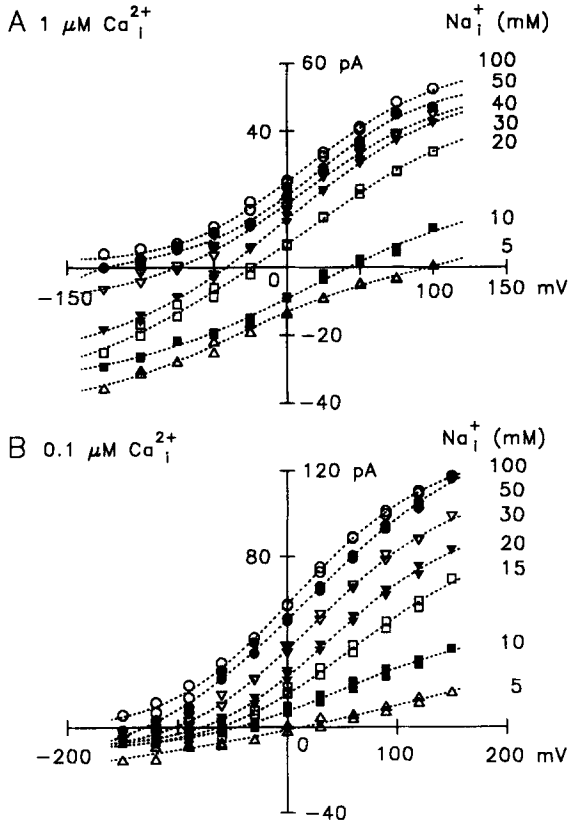

FIGURE 9. *I-V* relations of mixed exchange current. (*A*) *I-V* relations at different Na_i concentrations in the presence of 1 μM Ca_i with 2 mM Ca_o and 150 mM Na_o. Na_i concentrations are 100 mM (*open circles*), 50 mM (*filled circles*), 40 mM (*open inverted triangles*), 30 mM (*filled inverted triangles*), 20 mM (*open squares*), 10 mM (*filled squares*), and 5 mM (*open triangles*). (*B*) *I-V* relations at different Na_i concentrations in the presence of 0.1 μM Ca_i. Same pipette solution as in *A*, in a different patch. Na_i concentrations are 100 mM (*open circles*), 50 mM (*filled circles*), 30 mM (*open inverted triangles*), 20 mM (*filled inverted triangles*), 15 mM (*open squares*), 10 mM (*filled squares*), and 5 mM (*open triangles*).

In Fig. 9, *A* and *B*, results are presented with seven different Na_i concentrations. The two data sets are from different experiments. In Fig. 9 *A* with 1 μM Ca_i, it is first striking that *I-V* relations with 5, 10, and 20 mM Na_i are almost linear. The apparent reversal potential shifts from about +100 mV with 5 mM Na_i to +40 mV with 10 mM Na_i, and further to negative potentials at the higher Na_i concentrations. Note that the *I-V* relations at high Na_i concentrations tend to saturate at positive potentials. In Fig. 9 *B* with 0.1 μM Ca_i, the relative magnitude of inward exchange current is greatly reduced, and the reversal with 5 mM Na_i takes place at ~0 mV. A clear

saturation tendency with depolarization is observed with Na_i concentrations of >20 mM.

Fig. 10 shows plots of the reversal potential measurements against the Na_i concentrations. Open circles are with 1 μM Ca_i and filled circles are with 0.1 μM Ca_i. The solid lines are the expected results for perfect three-to-one stoichiometry. This result is consistent with previous results (Ehara, Matsuoka, and Noma, 1989). While the results are reasonably close to the three-to-one line, it is notable that the measured reversal potentials are consistently ~15 mV more positive than predicted. The largest discrepancy is 25 mV with 1 μM Ca_i.

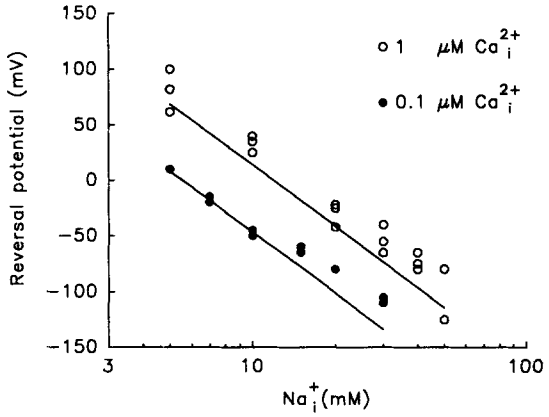

FIGURE 10. Reversal potentials of the exchange current. Reversal potentials are plotted against Na_i concentration in semilogarithmic fashion. Same protocol as in Fig. 9. Ca_i concentrations are 1 μM (*open circles*, $n = 3$) and 0.1 μM (*filled circles*, $n = 2$). Solid lines are predicted equilibrium potentials from three-to-one sodium-calcium exchange.

The Exchange Current I-V: Model Fits

It is noted first that the E4 and E8 models reproduce the *I-V* relations of the exchange current as just described equally well. Fig. 11 shows the *I-V* relations of the E8 model for the outward exchange current (*A* and *B*), inward exchange current (*C* and *D*), and mixed exchange currents (*E* and *F*). It is reminded that >20 other experiments have been fitted simultaneously, so that experimental variability is reflected in deviation of the concentration dependencies from the experimental data. Fig. 11 *A* gives results for variation of the Na_i concentration on outward current, and Fig. 11 *B* gives results for variation of the Ca_o concentration. The concentration dependencies, shapes of outward current *I-V* relations, and changes of shape with ion concentration changes are all well reproduced.

Fig. 11, *C* and *D* show the model fits for the Ca_i and Na_o concentration dependencies, respectively, of the *zero-trans* inward exchange current *I-V* relations. First, it is apparent in Fig. 11 *C* that there is some discrepancy in the Ca_i dependence of these results to the average results in the data base. The exchanger in this patch has an ~25% lower affinity to Ca_i than the average. The slopes and shapes of the *I-V* relations are, however, very well described by the E8 model. In Fig. 11 *D*, the Na_o dependence of the inward *I-V* relations is given with the E8 model. The shapes and Na_o dependence of the *I-V* relations are very accurately reproduced. Note that in the model, as in experiments, an increase of Ca_i from 6 μM to 1.4 mM results in no increase of inward current in the presence of 50 mM Na_o.

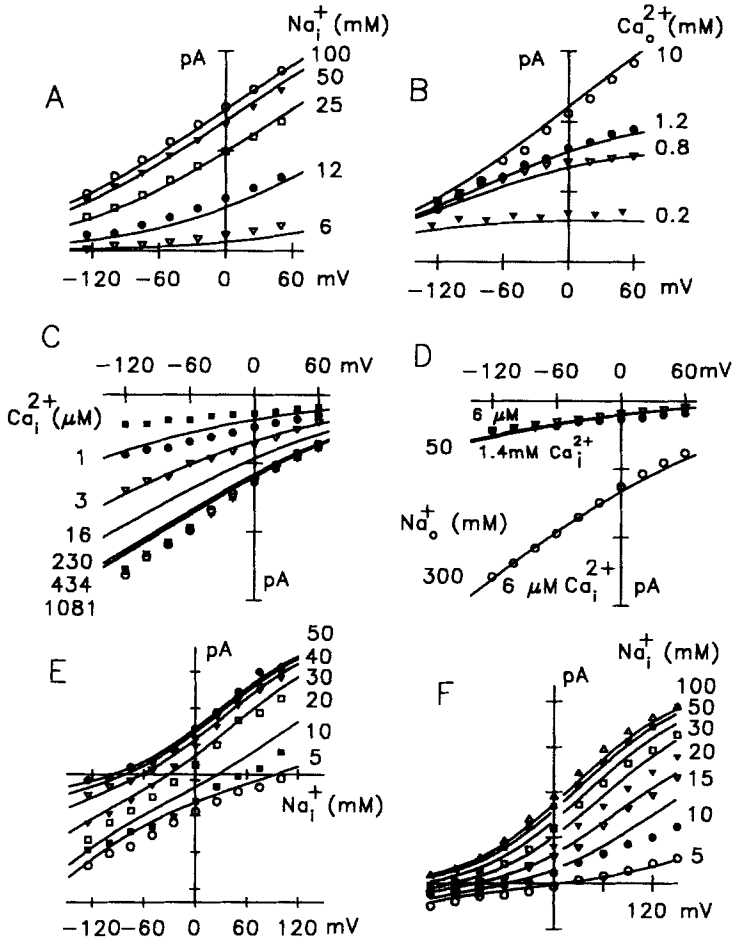

FIGURE 11. Simulated exchange currents with the E8 model. Symbols are experimental results and solid lines are the results of simulations. Conditions for simulations are the same as those of the corresponding experimental results. (*A*) Results of the outward exchange current with the E8 model for Na_i concentrations of 6 (*open inverted triangles*), 12 (*filled circles*), 25 (*open squares*), 50 (*filled inverted triangles*), and 100 mM (*open circles*). Experimental data from Fig. 4. (*B*) Results of the outward current for Ca_o concentrations of 0.2 (*filled inverted triangles*), 0.8 (*open inverted triangles*), 1.2 (*filled circles*), and 10 mM (*open circles*). Data from Fig. 6. (*C*) Simulation of the inward exchange current with the E8 model for Ca_i concentrations of 1 (*filled squares*), 3 (*filled circles*), 16 (*open inverted triangles*), 230 (*filled inverted triangles*), 434 (*open squares*), and 1,080 μM (*open circles*). 150 mM Na_o. Data from Fig. 7. (*D*) Simulation of the inward current for Na_o concentrations of 50 and 300 mM (*open circles*). Two Ca_i concentrations are given with 50 mM Na_o (6 μM [*open inverted triangles*] and 1.4 mM [*filled circles*]). Data from Fig. 8. (*E*) Simulation of the mixed exchange current of the E8 models. Na_i concentrations are 50 (*filled circles*), 40 (*open inverted triangles*), 30 (*filled inverted triangles*), 20 (*open squares*), 10 (*filled squares*), and 5 mM (*open circles*), as indicated. 1 μM Ca_i. Data from Fig. 9 *A*. (*F*) Results of simulations of mixed exchange current at 0.1 μM Ca_i. Data from Fig. 9 *B*. Na_i concentrations from top to bottom are 100 (*open triangles*), 50 (*filled squares*), 30 (*open squares*), 20 (*filled inverted triangles*), 15 (*open inverted triangles*), 10 (*filled circles*), and 5 mM Na_i (*open circles*).

In Fig. 11, *E* and *F*, the *I-V* relations of the mixed currents are reconstructed by the E8 model, with 1 and 0.1 μM Ca_i, respectively. As noted previously, the experimental results show some discrepancy from the perfect three-to-one stoichiometry of the model. The shapes of the *I-V* relations with both 1 and 0.1 μM free calcium are remarkably well described by the E8 model.

Comparison of the E2 and E8 Models

The simplest possible two-state models of sodium-calcium exchange with one electrogenic step during sodium translocation (Läuger, 1987; Hilgemann, 1988), as well as with partitioning of part of electrogenicity to the calcium translocation reaction (Niggli and Lederer, 1991), encounter a number of problems in accounting for our data base: (*a*) *I-V* relations tend to saturate too strongly at extremes of

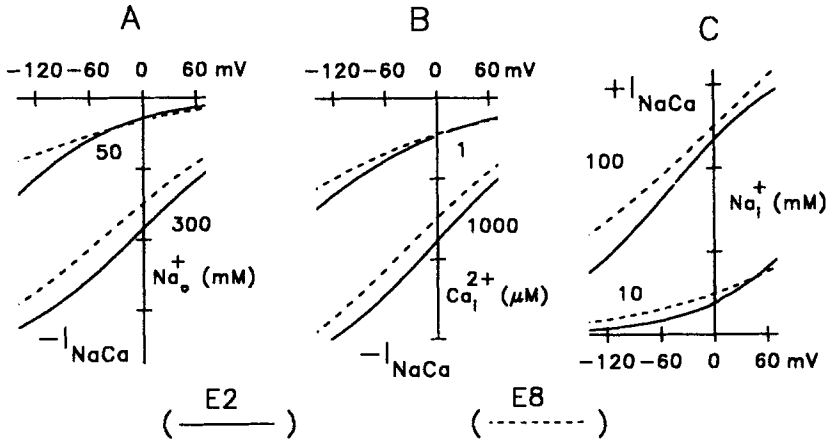

FIGURE 12. Difference between the E2 and E8 models. Results with the E2 (*solid lines*) and E8 models (*dotted lines*) are presented. (*A*) *I-V* relations of the inward exchange current at 50 and 300 mM Na_o with 0 mM Ca_o, 0 mM Na_i, and 1 mM Ca_i. (*B*) *I-V* relations of the inward exchange current at 1 and 1,000 μM Ca_i with 0 mM Ca_o, 150 mM Na_o, and 0 mM Na_i. (*C*) *I-V* relations of the outward exchange current at 10 and 100 mM Na_i with 10 mM Ca_o, 0 mM Na_o, and 0 μM Ca_i.

potential; (*b*) *I-V* relations change shape too strongly with changes of ion concentrations; in particular, the degree of steepening of *I-V* relations with reduction of ion concentrations is unrealistic; and (*c*), the slopes of *I-V* relations become too steep under one condition or another, depending on the detailed assumptions used. The E2 model overcomes some of these problems, but only partially.

Fig. 12 illustrates the general problems by comparing the best-fit simulation results of the E2 model with the E8 model. Dotted curves in Fig. 12 are the results of the E8 model, and solid curves are the results of the E2 model. Fig. 12 *A* shows the *I-V* relations of inward exchange current at 50 and 300 mM Na_o. With the E2 model, the slope of the *I-V* relation becomes too steep at low extracellular Na concentrations. Because there are multiple voltage-dependent occlusion steps in the Na translocation process of the E8 model, the *I-V* relations change their shape relatively little with

reduction of Na_o. Success of the E8 model depends critically on the placement of voltage-dependent steps *between* Na binding steps, not before Na binding or after complete Na loading. It is not possible, for example, to overcome the indicated problems by subdividing the translocation of calcium or the fully sodium-loaded exchanger into multiple steps. As concentrations are lowered in that case, and thereby the entrance rate into the multi-step ion translocation process is decreased, the overall translocation process behaves increasingly like a single, large step.

Fig. 12 *B* shows the *I-V* relations of inward exchange current at 1 and 1,000 μM Ca_i. With the E2 model, the slope of *I-V* relations becomes too steep at low Ca_i. This is because the E2 model is forced to place too large a voltage dependence on Ca occlusion from the cytoplasmic side. In this way, the model avoids a too steep voltage dependence at high Na_i concentrations, where the *I-V* slopes are determined largely by the voltage dependence of the sodium translocation pathway.

Fig. 12 *C* presents the *I-V* relations of the outward exchange current at 10 and 100 mM Na_i. The most important problem has already been outlined. The E2 model cannot accurately reproduce the shape of *I-V* relations in the low Na_i concentration

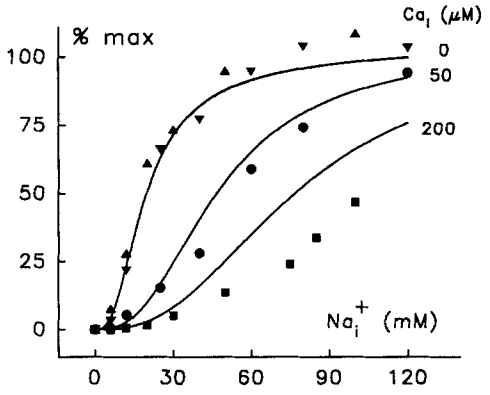

FIGURE 13. Inhibition of the outward current by Ca_i at 0 mV. Data are from two experiments and are normalized to the maximum current in the absence of Ca_i. Two controls in the absence of Ca_i (*filled triangles, filled inverted triangles*) and normalized currents in the presence of 50 μM (*filled circles*) and 200 μM (*filled squares*) Ca_i are plotted against Na_i concentration. Solid curves are the relations predicted by the E4 model.

range. The *I-V* relation at 10 mM is too steep. For the Ca_o dependencies of *I-V* relations (not shown), each of the models reproduces the ion dependencies and shape changes upon reduction of Ca_o concentration equally well.

In subsequent figures, results of the E4 model are given with experimental results. The results using the E8 model were at least as accurate, and in many cases somewhat more accurate, than those of the E4 model. It is pointed out that the E4 model formulation used does not include voltage dependence of Ca occlusion from the extracellular side as a variable. Nevertheless, it fits the relevant data equally well to the other models that associate the occlusion of calcium from the extracellular side with a small positive charge movement.

Cytoplasmic Ion Interactions: Competitive and Noncompetitive Components

Fig. 13 shows the effect of Ca_i on the Na_i dependence of the outward exchange current at 0 mV. The results are from two experiments, normalized to the maximum current obtained in the absence of Ca_i as 100%. Control results in the absence of Ca_i

from both experiments (triangles and inverted triangles), results from one experiment with 50 μM Ca_i (circles), and results from the other experiment with 200 μM Ca_i (squares) are shown. At 50 μM Ca_i, the current–Na_i concentration relationship is shifted to higher Na_i concentrations with no change of the maximum. At 200 μM Ca_i, the relationship is shifted further to the right without obvious decrease in maximum current up to 100 mM Na_i. Note that this is a linear concentration plot, and the decrease of slope does not reflect a decrease of Hill slope. The solid curves in this figure are the relationships predicted from the best fit of the E4 model.

While the results for the outward current (Fig. 13) can be well accounted for by ion binding equations with competitive sodium-calcium interactions, the equivalent results for inward current described in Fig. 14 are more complex. Results in Fig. 14 *A*

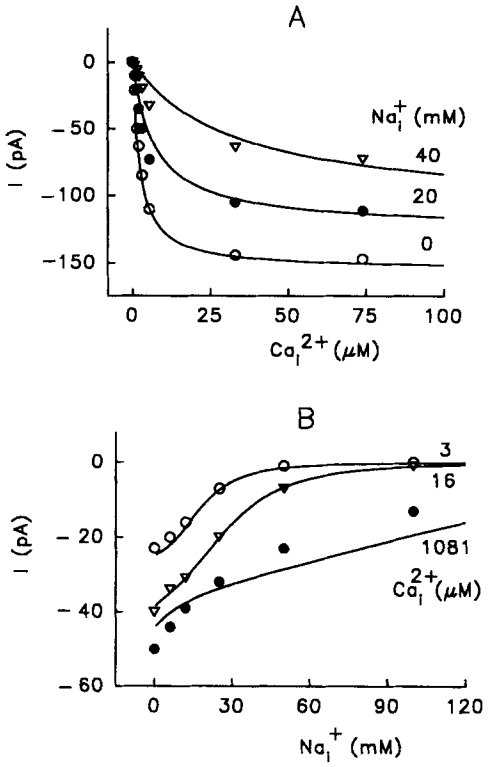

FIGURE 14. Inhibition of the inward exchange current by Na_i at 0 mV. Na_o concentration is 150 mM and Ca_o concentration is 0 mM. (*A*) Ca_i dependence of the inward exchange current at different Na_i. Amplitudes of the inward exchange current at 0 (*open circles*), 20 (*filled circles*), and 40 mM (*open inverted triangles*) Na_i concentrations in a patch are plotted against Ca_i concentration. (*B*) Concentration dependence of the inhibition of the inward current by Na_i. Amplitudes of the inward exchange current activated by 3 μM (*open circles*), 16 μM (*open inverted triangles*), and 1.08 mM (*filled circles*) Ca_i are plotted against Na_i concentration. Solid curves in both panels are relations predicted by the E4 model.

give the Ca_i dependence of inward current in the absence of Na_i (open circles) and in the presence of 20 mM (filled circles) and 40 mM (triangles) Na_i. While there is a shifting of the Ca_i dependence to higher Ca_i concentrations, there is also a strong reduction of the maximum current obtained at high Ca_i concentrations. Fitted to Hill equations, the results at 0, 20, and 40 mM Na_i gave K_h values of 2.4, 3.4, and 6.6 mM, respectively, and I_{max} values of −150, −111, and −74.1 pA, respectively.

Results in Fig. 14 *B* show the concentration dependence of inhibition of the inward current by Na_i at three different Ca_i concentrations. Data are at 3 μM (open circles), 16 μM (triangles), and 1.08 mM (filled circles) Ca_i concentration. At 3 μM Ca_i, the

inhibition by Na_i has an S shape that can be well fit by a Hill coefficient of 2.1 (see Methods in Hilgemann et al., 1992*b* for the modified Hill equation used). Half-inhibition occurs at 16.2 mM Ca_i, the S shape decreases and the inhibition curve becomes monotonic. The Hill coefficient is 1.1 and the half maximal Na_i concentration is 37.3 mM. The model-based half-maximal inhibition by Na_i is shifted to a higher Na_i concentration by only a factor of 2.8 for a 360-fold change of Ca_i (i.e., for 3 μM to 1.08 mM Ca_i).

These experimental results are well accounted for by the assumption that one Na can bind to the carrier, which has already bound one Ca ion on the cytoplasmic side. Solid lines in Fig. 14, as well as in Fig. 13, are the relationships predicted by the E4

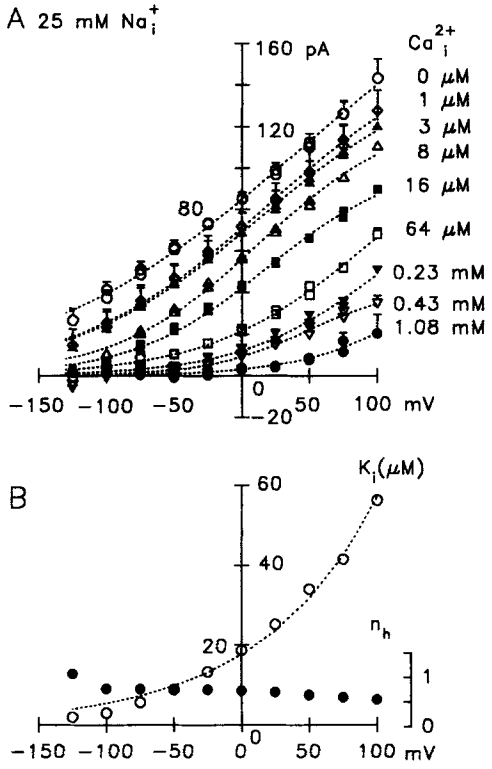

FIGURE 15. Inhibition of the outward exchange current by Ca_i in *I-V* relations. Na_o concentration is 0 mM and Ca_o concentration is 8 mM. (*A*) *I-V* relations at 25 mM Na_i and different Ca_i concentrations: 0 μM (*open circles*), 1 μM (*open diamonds*), 3 μM (*filled triangles*), 8 μM (*open triangles*), 16 μM (*filled squares*), 64 μM (*open squares*), 0.23 mM (*filled inverted triangles*), 0.43 mM (*open inverted triangles*), and 1.08 mM (*filled circles*). Data are shown as mean + SD (n = 4–6 at each Ca_i concentration). (*B*) Voltage dependence of the K_i and n_h at 25 mM Na_i. K_i (*open circles*) and n_h (*filled circles*) values that fitted data in *A* to the modified Hill equation are plotted against membrane potential. A scale for n_h is placed at the right side of the panel. The dotted line is a fitted Boltzmann relation; $K_i = 17.5 \cdot e^{0.32 \cdot Em/26.6}$.

model, which incorporates this assumption. At high Ca_i concentrations (1.08 mM in Fig. 14 *B*), inhibition of the inward current is brought about primarily by Na binding at the third site, rather than by competition with calcium at the first binding site.

Cytoplasmic Ion Interactions: The Outward Exchange Current I-V

The voltage dependencies of the interactions between Na_i and Ca_i are presented in Figs. 15–19. Figs. 15 and 16 present the effect of Ca_i on the *I-V* relations of the outward exchange current. Results in Fig. 15 are with 25 mM Na_i and 8 mM Ca_o. At 25 mM Na_i the outward exchange current is inhibited by 1, 3, and 8 μM Ca_i in a potential-sensitive fashion. The inhibition at negative potentials is a much larger

fraction of the exchange current than at positive potentials, and the *I-V* relations gain in curvature as the Ca_i concentration is increased. Above 64 μM Ca_i the *I-V* relations essentially scale down as Ca_i is increased, and 1.08 mM Ca_i inhibits >95% of the outward current at 0 mV.

Amplitudes of the current at different potentials were plotted against Ca_i concentration and fitted to a modified Hill equation (see Methods in Hilgemann et al., 1992*b*; data not shown). The fitted Ca_i concentrations giving half-maximal inhibition (K_i, open circles) are plotted in Fig. 15 *C*, together with the slope values (n_h, filled circles) fitted with the Hill equation. The K_i for Ca_i increases markedly from 1.9 μM

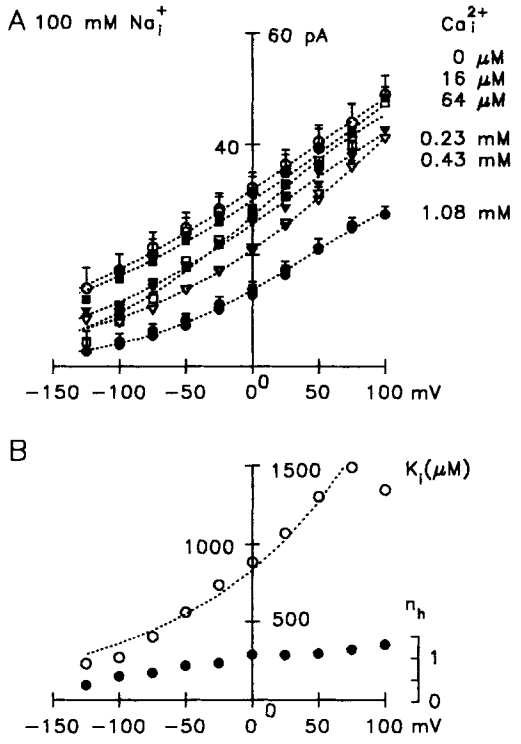

FIGURE 16. (*A*) *I-V* relations at 100 mM Na_i and different Ca_i concentrations: 0 μM (*open circles*), 16 μM (*filled squares*), 64 μM (*open squares*), 0.23 mM (*filled inverted triangles*), 0.43 mM (*open inverted triangles*), and 1.08 mM (*filled circles*). Data are shown as mean + SD (n = 4–6 at each Ca_i concentration). (*B*) Voltage dependence of the K_i and n_h at 100 mM Na_i. Data from *A* are plotted in the same manner as in Fig. 15 *B*. A fitted Boltzmann relation is $K_i = 833 \cdot e^{0.20 \cdot EM/26.6}$.

at −125 mV to 56 μM at +100 mV. Fitted to a Boltzmann relation, these results have a slope value of 0.32. n_h values fall between 0.5 and 1.1 and tend to decrease with depolarization.

Fig. 16 *A* shows the same sequence of experiments with 100 mM Na_i. The shape changes obtained by inhibition with 16 μM to 1.08 mM Ca_i are very similar to those at 25 mM Na_i, showing a voltage-dependent inhibition. However, the fractional inhibition is greatly decreased in comparison to results with 25 mM Na_i. At 0 mV the current is inhibited by ~60%, by 1.08 mM Ca_i.

Fig. 16 *B* presents K_i (open circles) and n_h (filled circles) values in the presence of 100 mM Na_i fitted to a modified Hill equation. The K_i again shows a voltage-dependent increase, from 232 μM at −125 mV to 1.5 mM at +75 mV. The slope

value of the fitted Boltzmann equation (dotted line) is 0.20. The corresponding fitted n_h values increase with depolarization from ~0.4 at −125 mV to 1.4 at +100 mV.

Cytoplasmic Ion Interactions: The Inward Exchange Current I-V

Voltage dependencies of the interaction of Na_i and Ca_i were also studied for the inward exchange current. Figs. 17 and 18 present the inhibition of inward exchange current by Na_i in *I-V* relations. The results are with 150 mM Na_o and no Ca_o. Fig. 17 *A* is with 3 μM Ca_i, and Fig. 17 *B* is with 1.08 mM Ca_i. With 3 μM Ca_i (*A*), Na_i inhibits the inward current much more strongly at positive potentials than at negative

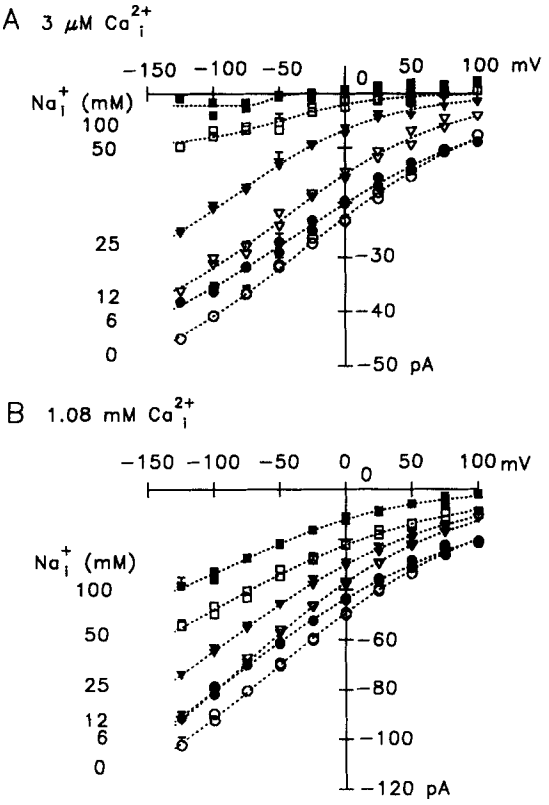

FIGURE 17. The inhibition of the inward exchange current by Na_i in *I-V* relations. Na_o concentration is 150 mM and Ca_o concentration is 0 mM. Same patch in *A* and *B*. Data are shown as mean + SD (n = 4–6 at each Na_i concentration). (*A*) *I-V* relations in the presence of 3 μM Ca_i and different Na_i concentrations: 0 (*open circles*), 6 (*filled circles*), 12 (*open inverted triangles*), 25 (*filled inverted triangles*), 50 (*open squares*), and 100 mM (*closed squares*). (*B*) *I-V* relations in the presence of 1.08 mM Ca_i and different Na_i. Same symbols as in *A*.

potentials. Accordingly, the *I-V* relations gain in curvature as the Na_i concentration is increased. With 1.08 mM Ca_i (*B*), the inhibition is substantially decreased. The changes in the shape of *I-V* relations are somewhat less pronounced, although similar to those with 3 μM Ca_i. Note that the results in this figure are all from the same patch.

The results from Fig. 17 are plotted in Fig. 18 in the concentration domain (symbols) and are fitted to the modified Hill equation (dotted lines) in Fig. 18, *A* and *B*, respectively, for results with 3 μM and 1.08 mM Ca_i. The K_i for Na_i with 3 μM Ca_i (Fig. 18 *C*) decreases from 28.9 mM at −125 mV to 12.9 mM at +100 mV. The slope

(n_h) of the modified Hill equation tends to increase with depolarization, but the values cluster around 2. With 1.08 mM Ca_i (Fig. 18 *D*), the K_i's for Na_i values are somewhat more than doubled and similarly decrease with depolarization. Notably, n_h values are markedly decreased in comparison to Fig. 18 *C* to close to 1 at all

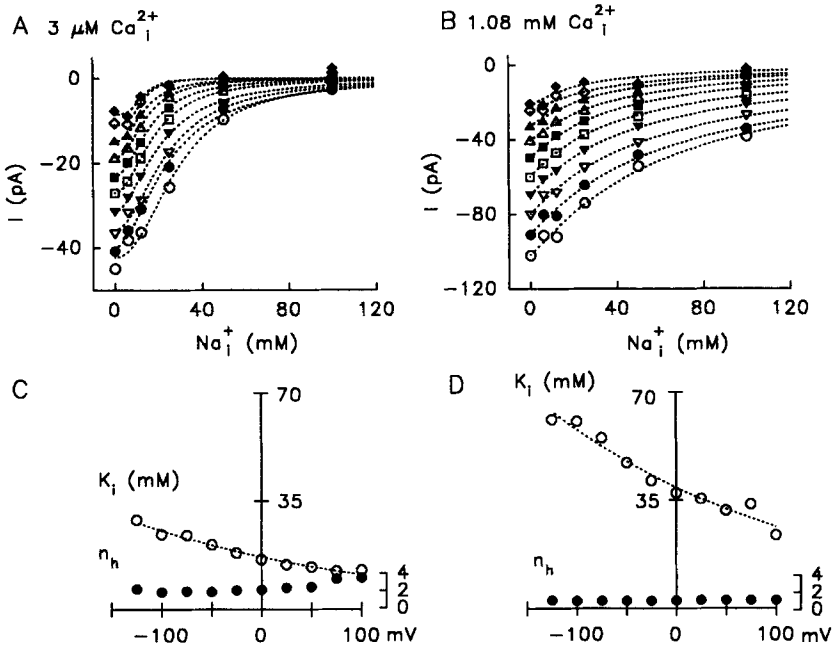

FIGURE 18. Voltage dependence of the inhibition of the inward exchange current by Na_i. (*A*) Concentration dependence of the inhibition by Na_i in the presence of 3 μM Ca_i at different membrane potentials. Data are from Fig. 17 *A*. Amplitudes of the current are plotted against Na_i concentrations: −125 (*open circles*), −100 (*filled circles*), −75 (*open inverted triangles*), −50 (*filled inverted triangles*), −25 (*open squares*), 0 (*filled squares*), 25 (*open triangles*), 50 (*filled triangles*), 75 (*open diamonds*), and 100 mV (*filled diamonds*). (*B*) Concentration dependence of the inhibition by Na_i in the presence of 1.08 mM Ca_i at different membrane potentials. Data are from Fig. 17 *B*. Same symbols as in *A*. Dotted lines in both *A* and *B* are fitted modified Hill relations. (*C*) Voltage dependence of K_i and n_h in the presence of 3 μM Ca_i. K_i (*open circles*) and n_h (*filled circles*) from *A* are plotted against membrane potentials. A scale for n_h is placed at the right side of the panel. The dotted line is a fitted Boltzmann relation; $K_i = 17.0 \cdot e^{-0.11 \cdot Em/26.6}$. (*D*) Voltage dependence of K_i and n_h at 1.08 mM Ca_i. Data are from *B* and are plotted in the same manner as in *C*. A fitted Boltzmann relation is $K_i = 40.0 \cdot e^{-0.1 \cdot Em/26.6}$.

membrane potentials. Slope factors for the fitted Boltzmann equations with 3 μM and 1.08 mM Ca_i are −0.11 and −0.10, respectively.

Finally, a comparison between these results and results with outward current is noteworthy. Here, a 360-fold increase of Ca_i concentration increases the apparent K_i for Na_i by less than threefold (2.3-fold at 0 mV, K_i = 16.2 mM at 3 μM Ca_i and 37.3 mM at 1.08 mM Ca_i). In the results for outward current, an increase of Na_i

concentration by fourfold was found to increase the apparent K_i for Ca_i by ~50-fold (18.6 mM at 25 mM Na_i and 885 mM at 100 mM Na_i, at 0 mV).

Cytoplasmic Ion Interactions: Model Fits of I-V Relations

Fig. 19 shows experimental data points and the predictions of the E4 model for the results on Na_i and Ca_i interactions (solid lines). Results for the outward current are presented in Fig. 19, *A* and *B*, and results for the inward current are shown in Fig. 19, *C* and *D*. Fig. 19 *A* shows predicted *I-V* relations at 25 mM Na_i concentration in the absence of Ca_i (experimental data; open circles), and in the presence of 16 μM (filled circles) and 234 μM Ca_i (triangles). Fig. 19 *B* shows the predicted results for 100 mM Na_i. Data are without Ca_i (open circles), and with 64 μM (filled circles) and 1.08 mM (triangles) Ca_i. While there is some discrepancy in the concentration dependence at high Ca_i concentrations in Fig. 19 *A*, the changes of *I-V* position and shape are very well predicted by the model.

Fig. 19 *C* shows the predicted inward current with 3 μM Ca_i. Na_i concentrations are 0 mM (open circles), 25 mM (filled circles), and 50 mM (triangles). The model fits the experimental results in considerable detail. Note that the inward current at +100 mV can be inhibited by ~95% when the current at −120 mV is inhibited by only 40%. Fig. 19 *D* shows the predicted inward current with 1.08 mM Ca_i. Na_i concentrations are 0 mM (open circles), 25 mM (filled circles), and 100 mM (triangles). While there is some discrepancy in this fit with respect to the concentration–effect relation, the description of shape changes in the *I-V* relation as Na_i is increased is clearly excellent.

DISCUSSION

The experiments described in this article provide detailed information about the steady-state ion and voltage dependencies of the chymotrypsin-deregulated exchanger in guinea pig sarcolemma. We have presented the data with a perspective on the exchange mechanism by fitting the data base to different models of the exchange cycle. The data set is admittedly not comprehensive. In particular, information about the interactions of Na_o and Ca_o, and their voltage dependencies are not available for the deregulated exchanger. We find some differences from previous data in giant patches, but within the time frame of this study the various types of results presented were reproducible and consistent in good detail. The reliability of the techniques and protocols used has been tested extensively, and it is improved over those used in previous studies. On this basis, our use of the data set to test the viability of hypothetical exchange models appears well justified.

Relationships to Previous Data: Variable Results

Chymotrypsin treatment of the exchange system greatly reduces variabilities and time-dependent changes of exchange function in experiments with giant cardiac membrane patches. As pointed out in Results, we have nevertheless been impressed by some variabilities in experimental results on voltage dependencies of the deregulated exchange current over a 2-yr period. According to our criteria for isolating the exchange current, the differences must reflect genuine differences in the functional status of the exchanger in different sets of experiments. Factors that might be important include (*a*) different enzymes and exact protocols used for cell isolation

and storage, (*b*) different species used in some work (e.g., guinea pig vs. rabbit), (*c*) differences in exchange function related to hormonal or other long-term variables of the animals used, and (*d*) differences in the extent of proteolysis by chymotrypsin, assuming that this treatment affects exchange function under conditions we have not tested to date.

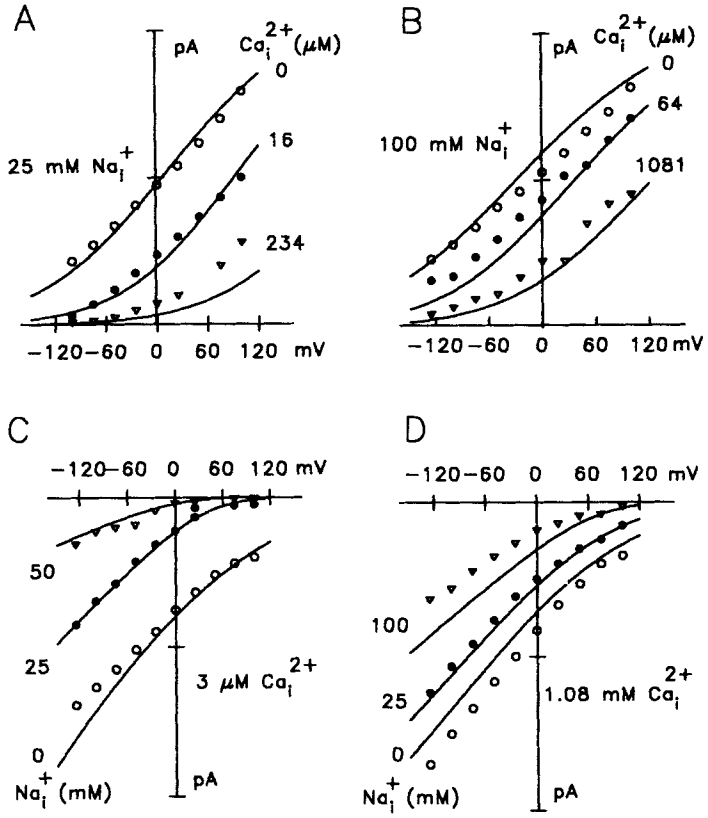

FIGURE 19. E4 model predictions for conditions of mixed ions on the cytoplasmic side. Solid curves in all panels demonstrate results predicted from the E4 model. (*A*) The *I-V* relations of the outward exchange current activated by 25 mM Na_i at different Ca_i concentrations. Data from Fig. 15 *A*: 0 (*open circles*), 16 (*filled circles*), and 234 μM Ca_i (*open inverted triangles*), as indicated. (*B*) The *I-V* relations of the outward current activated by 100 mM Na_i at different Ca_i concentrations. Data from Fig. 16 *A*: 0 μM (*open circles*), 64 μM (*filled circles*), and 1.08 mM Ca_i (*open inverted triangles*) as indicated. (*C*) The *I-V* relations of the inward exchange current activated by 3 μM Ca_i. Results are from Fig. 17 *A* with 0 (*open circles*), 25 (*filled circles*), and 50 mM Na_i (*open inverted triangles*) as indicated. (*D*) The *I-V* relations of the inward exchange current activated by 1.08 mM Ca_i. The results are for 0 (*open circles*), 25 (*filled circles*), and 100 mM Na_i (*open inverted triangles*) as in Fig. 17 *B*.

One striking difference between results in giant patches and whole cells, for which we have no explanation, is the very small effect of monovalent ions on outward exchange current in giant patches (Fig. 1) compared with whole myocytes (Gadsby et al., 1991). Other differences are pointed out in the subsequent discussion.

Ion Dependencies of Deregulated Exchanger: Competitive and Noncompetitive Ion Interactions

The basic ion dependencies of deregulated exchange current in giant patches (Fig. 3) are entirely consistent with results in intact myocytes (Kimura, Miyamae, and Noma, 1987; Miura and Kimura, 1989), insofar as equivalent data are available. The major missing piece for myocytes was the complete Ca_i dependence of the inward exchange current in the absence of cytoplasmic Na. With 150 mM Na_o, our K_h for Ca_i at 0 mV is ~5 μM. This is two- to fourfold lower than mean values obtained in cardiac vesicles (Reeves and Philipson, 1989). Apart from this quantitative difference, a qualitative difference from results with vesicles is our finding of a noncompetitive component of the interaction between Na and Ca on the cytoplasmic side. Although only a competitive interaction between Na and Ca was described in cardiac vesicles (Reeves and Sutko, 1983) and intact cardiac myocytes (Miura and Kimura, 1989), results similar to ours have been described for Ca efflux in the squid axon (Fig. 3 of Blaustein and Russell, 1975).

In all of the simulations presented, the pattern of competitive-noncompetitive interaction is accounted for by assuming that one Na ion can bind after binding of Ca on the cytoplasmic side. Although not supported by any other work, these results raise speculative possibilities that one Ca and one Na ion might be translocated slowly in a reaction leading to less than three-to-one stoichiometry, and/or that one Na ion could be transported separately from the other two in a pathway inaccessible to Ca. In any case, it will be important to study in more detail the sodium-calcium interactions from the extracellular side with respect to a possible noncompetitive interaction. It would be remarkable if a mixed ion binding configuration existed only from the cytoplasmic side.

A very important issue about ion binding that must be decided in simulations is whether the binding reactions can be treated as instantaneous. The relevant simulation result is that a significant time dependence of the binding reactions in relation to other cycle steps leads to noncompetitive behaviors for both exchange modes. Results are similar if there are time-dependent steps between ion binding reactions. Since a purely competitive behavior is found for the outward current from the cytoplasmic side, and mixed interactions are not described for the extracellular side, we assume that all binding sites for both Na and Ca are available on the empty carrier and that binding is very fast in relation to occlusion reactions. The time-dependent occlusion of one Na ion presumably does not generate the binding site for the next ion.

Confirmation of Consecutive Exchange Cycle

In the course of these measurements, no results or problems arose that might qualify previous conclusions that the cardiac sodium-calcium exchanger functions by a consecutive-type (ping-pong) mechanism (Khananshvili, 1990; Li and Kimura, 1990, 1991; Hilgemann et al., 1991*b*). An increase in the apparent cytoplasmic ion affinity was routinely verified whenever the counter-transported ion concentrations were decreased (Fig. 3). Over and above this confirmation, the successful simulation of a number of other results depends on the assumption of a consecutive cycle. Good examples are the changes of *I-V* shapes described for inhibition of exchange current

by the counter-transported ion on the cytoplasmic side (Fig. 19). These results are predicted qualitatively by simple two-state consecutive exchange models, and surprisingly, details of the assignment of voltage-dependent steps were not critical for a qualitative reconstruction of the data. The results were not predicted by any of the simultaneous models available to us (Hilgemann, 1988).

Shifts of Ion Dependencies and I-V Relations Confirm Voltage Dependence of the Sodium Translocation Pathway

In our present results, we have described under *zero-trans* conditions ion concentration-dependent changes in the voltage dependence of the exchanger, and vice versa, voltage-dependent changes in the ion concentration dependencies of exchange. The direction of each change measured is qualitatively consistent with the predictions of simple, two-state consecutive exchange models with voltage dependence placed on Na translocation (i.e., with movement of one positive charge through the membrane field during Na translocation), and the direction of each shift is opposite to that expected for the equivalent model with all voltage dependence placed on Ca translocation (i.e., with one negative charge movement placed on Ca translocation). For the Ca dependence of the exchanger, Khananshvili (1991) has described similar results with the exchanger incorporated into proteoliposomes. These results taken together strongly support the conclusion that electrogenicity in the cardiac sodium-calcium exchange cycle arises primarily within the sodium translocation pathway (Hilgemann et al., 1991*b*).

The same results are, however, also indicative of a more complex basis of electrogenicity in the exchange cycle. The voltage-dependent shifts of apparent affinity for Na and Ca are substantially smaller than those predicted by the simple models. The *I-V* relations, particularly the inward *I-V* relations, are less steep than predicted by the simple models. In addition, voltage dependence of the inward current can be considerable at low Ca_i concentrations, which contradicts the simple models. The *I-V* shape changes obtained in this study for changes of Na_o are notably much smaller than those described for the rod outer segment sodium-calcium, potassium exchanger (Lagnado, Cervetto, and McNaughton, 1988).

Independent of the basis of these complexities, it is clearly important that the presence of both Na and Ca on one membrane side, the cytoplasmic side in our experiments, strongly affects the shapes and slopes of *I-V* relations in the sense of a steepening. This may explain some of the variability observed in exchange current *I-V* relations described in intact myocytes, where control of cytoplasmic ion concentrations is limited (e.g., Kimura et al., 1987; Earm, Ho, and So, 1990; Bridge, Smolley, Spitzer, and Chin, 1991; Gadsby et al., 1991). On the basis of modeling, we predict that the presence of both ions on the extracellular side will also be important, independent of a possible secondary activating effect of extracellular monovalent cations. In intact myocytes, for example, the *I-V* relations of the outward exchange current decrease almost synchronously over 150 mV as the Ca_o concentration is decreased in the presence of 140 mM Na_o (Kimura et al., 1987; Ehara et al., 1989). The models presented closely predict this result (see Appendix).

The Basis of Electrogenicity: Narrow Access Channel Versus Ion Occlusion/Deocclusion Reactions

Two general principles have been widely discussed as the physical basis of electrogenicity of ion transporters. First, the net charge carried by binding sites and loaded ions may move through the electrical field during the occlusion and/or translocation of ions, and second, electrogenicity may arise during the binding of ions under the assumption that ions pass through a significant fraction of membrane field on approach to binding sites through a narrow access channel (for overview see Läuger, 1991; for recent discussion with respect to the exchanger, see McNaughton, 1991). The voltage-dependent changes of the K_h for both Na and Ca described in this article (Figs. 5, 6, and 7) are qualitatively consistent with the idea of narrow access channels for sodium on both membrane sides. The effects observed are small, however, and the changes are not specific to an access channel hypothesis, as demonstrated by our simulations.

For sodium, the incorporation of high resistance access channels into simulations invariably worsened data fits by generating larger effects of ion concentration changes on *I-V* relations than we have found experimentally. For calcium, a sizable voltage dependence of binding on either side gives rise to a major prediction that the slope of *I-V* relations should not only decrease, but should reverse its direction as calcium concentrations are reduced, giving rise to bell-shaped *I-V* relations (e.g., Läuger, 1987). Negative slopes either were not found or were extremely small with reduction of calcium on the extracellular side, and they were never found with reduction of calcium from the cytoplasmic side.

For the reasons discussed, we are forced to conclude that the bulk of electrogenicity in the sodium-calcium exchange cycle is related to the occlusion of ions by the exchanger, presumably associated with conformational changes of binding sites. We point out in this regard the strong precedent of work with the anion exchanger, indicating only slight effects of voltage in an ion transporter that can operate at turnover rates of $>100{,}000\ s^{-1}$ (Jennings, Schulz, and Allen, 1990). Clearly, substantial high-resistance access channels are not an essential physical property of ion transporters.

Location of Electrogenic Steps in Transport Cycle

While the *I-V* relations of sodium-calcium exchange current can be nearly exponential with slopes nearly as expected for a simple two-state carrier (e.g., Figs. 15, 16, and 17 with both Na and Ca on the cytoplasmic side), the *I-V* relations can also be nearly linear with approximate linearity extending over remarkably wide voltage ranges. Similarly, linear effects of membrane potential have been reported under ionic conditions close to ours in an ion flux study in squid axon (Allen and Baker, 1986*b*; results that were described well by the E8 model in simulations not presented), for measurements of inward exchange current in squid axon (DiPolo, Bezanilla, Caputo, and Rojas, 1985), for the cardiac exchanger incorporated into proteoliposomes (Khananshvili, 1991), and for the inward exchange current in intact myocytes in some reports (Niggli and Lederer, 1991) but not others (Kimura et al., 1987; Bridge et al., 1991; Hilgemann et al., 1991*b*).

As with ion permeation through channels (for references see Hille, 1992), it is demonstrated in our simulations that the electrogenicity of the exchange cycle can be broken down successfully into multiple steps. Up to seven steps improve simulations and a minimum of two sodium occlusion reactions and one calcium occlusion reaction are essential to allow accurate simulations. Relevant to these simulation results it has been suggested that a charge moving step can remain "hidden" in *I-V* relations if that step is very fast in relation to other cycle steps (Niggli and Lederer, 1991). While it is certainly possible to account for individual *I-V* relations in this way, our experience from modeling is that hidden electrogenic steps are invariably revealed when studying *I-V* relations over the wide range of conditions in our study.

Two details appear essential for reproducing our results: (*a*) The electrogenic steps in the Na translocation pathway must be separated from one another by Na binding reactions, rather than occurring as sequential translocation steps in the fully loaded configuration. This accounts for the fact that the slopes of *I-V* relations remain relatively shallow as Na concentrations are reduced, on both the extracellular side and the cytoplasmic side. (*b*) Ca occlusion/deocclusion on the cytoplasmic side, but not on the extracellular side, involves the movement of a small net negative charge (i.e., reflecting a negative binding site charge of slightly more than 2) into the membrane electrical field. This accounts for the fact that voltage dependence of the inward current is not entirely lost as Ca_i is reduced, in contrast to results for the outward current as Ca_o is reduced. As described in the Appendix, the assumption of a negative charge movement with occlusion of Ca from the cytoplasmic side predicts qualitatively the depolarization-dependent decrease of calcium-calcium exchange described by DiPolo and Beaugé (1990). Presumably, the negative charge movement of cytoplasmic calcium occlusion originates from the partial movement of electrical field across fixed negative charges toward the cytoplasmic mouth of the exchanger binding sites.

In previous work (Hilgemann et al., 1991*b*), an asymmetry of charge movement of Na translocation was suggested in the sense that occlusion on the extracellular side was voltage dependent while occlusion on the cytoplasmic side was not. This was consistent with a sidedness of the effects of Na concentration changes on *I-V* relations and later with the fact that voltage-dependent charge movements could be induced under specifically chosen conditions to orient the exchanger binding sites to the extracellular side in the presence of Na_o (Hilgemann, Philipson, and Nicoll, 1992*c*). In the present work, *I-V* shape was sensitive to changes in both Na_i and Na_o concentrations, which again underscores our impression of a degree of plasticity in the charge moving steps of the exchange cycle. According to our present understanding, the movement of one charge in the exchange cycle is subdivided into multiple steps involving rearrangements of binding sites and the different numbers and species of ions bound. In this light, rather subtle conformational changes of the exchanger and/or its charged environment might be expected to modify the detailed partitioning of voltage dependence between different steps and the exact amount of binding site charge that enters membrane field during ion translocation. The systematic identification of factors that influence this partitioning could provide an important handle on molecular determinants of electrogenicity in the cardiac sodium-calcium exchange cycle.

APPENDIX

Formulation of Models

In each of the models, Na binding is assumed to be instantaneous and to take place sequentially with competition of the first Na for Ca. On the cytoplasmic side, one Na ion can bind subsequent to one Ca ion, giving the Fcn binding site fraction in the following diagram. The Fcn fraction is omitted on the extracellular side.

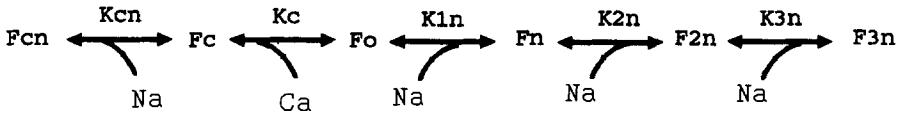

For the extracellular side, Kc_o, $K1n_o$, $K2n_o$, and $K3n_o$ are the dissociation constants for the respective binding reactions, and Fc_o and $F3n_o$ are the fractions of binding sites occupied by Ca and three Na ions, respectively.

The E8 model. With the designation of C_o and N_o as the extracellular free Ca and Na concentrations, respectively, and with the calculation of a common denominator, D_o,

$$D_o = \frac{C_o}{Kc_o} + 1 + \frac{N_o}{K1n_o} + \frac{N_o^2}{K1n_o \times K2n_o} + \frac{N_o^3}{K1n_o \times K2n_o \times K3n_o} \tag{1}$$

$$Fc_o = \left(\frac{C_o}{Kc_o}\right)\Big/D_o \tag{2}$$

$$F3n_o = \left(\frac{N_o^3}{K1n_o \times K2n_o \times K3n_o}\right)\Big/D_o \tag{3}$$

These fractions apply to the E_3 state in the E8 model.

For the cytoplasmic side, Kcn_i, Kc_i, $K1n_i$, $K2n_i$, and $K3n_i$ are the dissociation constants for the respective binding reactions, and Fc_i and $F3n_i$ are the fractions of binding sites occupied by Ca alone and by three Na ions, respectively. With designation of C_i and N_i as the free cytoplasmic Ca and Na concentrations, respectively, and calculation of a common denominator, D_i,

$$D_i = \frac{C_i}{Kc_i} + \frac{C_i \times N_i}{Kc_i \times Kcn_i} + 1 + \frac{N_i}{K1n_i} + \frac{N_i^2}{K1n_i \times K2n_i} + \frac{N_i^3}{K1n_i \times K2n_i \times K3n_i} \tag{4}$$

$$Fc_i = \frac{C_i}{Kc_i}\Big/D_i \tag{5}$$

$$F3n_i = \left(\frac{N_i^3}{K1n_i \times K2n_i \times K3n_i}\right)\Big/D_i \tag{6}$$

These fractions apply to the E_1 state.

Additional preliminary calculations are required for the total fraction of binding sites in the E_1 and E_3 states whose first Na binding site is occupied by Na ($F'1n_i$ and $F'1n_o$) and therefore is available for the first Na occlusion reaction:

$$F'1n_i = \left(\frac{N_i}{K1n_i} + \frac{N_i^2}{K1n_i \times K2n_i} + \frac{N_i^3}{K1n_i \times K2n_i \times K3n_i}\right)\Big/D_i \tag{7}$$

$$F'1n_o = \left(\frac{N_o}{K1n_o} + \frac{N_o^2}{K1n_o \times K2n_o} + \frac{N_o^3}{K1n_o \times K2n_o \times K3n_o}\right) \Big/ D_o \tag{8}$$

Also, preliminary calculations are required for the total fractions of E_8 and E_4 binding sites whose second Na binding site is occupied by Na ($F'2n_i$ and $F'2n_o$):

$$F'2n_i = \left(\frac{N_i}{K2n_i} + \frac{N_i^2}{K2n_i \times K3n_i}\right) \Big/ \left(1 + \frac{N_i}{K2n_i} + \frac{N_i^2}{K2n_i \times K3n_i}\right) \tag{9}$$

$$F'2n_o = \left(\frac{N_o}{K2n_o} + \frac{N_o^2}{K2n_o \times K3n_o}\right) \Big/ \left(1 + \frac{N_o}{K2n_o} + \frac{N_o^2}{K2n_o \times K3n_o}\right) \tag{10}$$

and finally, for the total fractions of the E_7 and E_5 states whose third Na binding site is occupied by Na ($F'3n_i$ and $F'3n_o$):

$$F'3n_i = \left(\frac{N_i}{K3n_i}\right) \Big/ \left(1 + \frac{N_i}{K3n_i}\right) \tag{11}$$

$$F'3n_o = \left(\frac{N_o}{K3n_o}\right) \Big/ \left(1 + \frac{N_o}{K3n_o}\right) \tag{12}$$

Q_n is the fractional charge movement taking place with each of the Na occlusion reactions, Q_{ci} is the fractional charge movement taking place with occlusion of cytoplasmic Ca, and Q_{co} is the fractional charge movement taking place with occlusion of extracellular Ca. Q_n was simulated as a positive charge and Q_c as a negative charge movement through the membrane field in the direction of ion occlusion. During the preliminary calculations of each cycle in the fitting procedure, the constraint of one charge movement was enforced,

$$Q_{ci} + Q_{co} + 6 \times Q_n = 1 \tag{13}$$

and here as well as in the other models, microscopic reversibility was enforced on the dissociation constants at each cycle calculation,

$$\frac{Kc_i \times K1n_o \times K2n_o \times K3n_o}{Kc_o \times K1n_i \times K2n_i \times K3n_o} = 1 \tag{14}$$

The rate constants for the model are designated by subscripts giving the direction of the transition (e.g., k_{81} designates the rate constant for the E8 to E1 transition). The maximum rate of each step of the cycle at 0 mV, k_x, was arbitrarily set to 1,000 s^{-1} during the fitting procedure. This is a pseudo-variable, since each experiment was fitted with a scaler variable. To obtain fully activated turnover rates of the cycle of 5,000 s^{-1}, as predicted previously (Hilgemann et al., 1991*b*), k_x values of $\sim 10^5$ s^{-1} must be assumed. With membrane potential designated as Em and with $2 \cdot RT/F = 53$ mV,

$$k_{12} = k_x \times Fc_i \times e^{-Qci \times Em/53} \tag{15}$$

$$k_{21} = k_x \times e^{Qci \times Em/53} \tag{16}$$

$$k_{23} = k_x \times e^{-Qco \times Em/53} \tag{17}$$

$$k_{32} = k_x \times Fc_o \times e^{Qco \times Em/53} \tag{18}$$

$$k_{34} = k_x \times F'1n_o \times e^{-Qn \times Em/53} \tag{19}$$

$$k_{43} = k_x \times e^{Qn \times Em/53} \tag{20}$$

$$k_{45} = k_x \times F'2n_o \times e^{-Qn \times Em/53} \quad (21)$$

$$k_{54} = k_x \times e^{Qn \times Em/53} \quad (22)$$

$$k_{56} = k_x \times F'3n_o \times e^{-Qn \times Em/53} \quad (23)$$

$$k_{65} = k_x \times e^{Qn \times Em/53} \quad (24)$$

$$k_{67} = k_x \times e^{-Qn \times Em/53} \quad (25)$$

$$k_{76} = k_x \times F'3n_i \times e^{Qn \times Em/53} \quad (26)$$

$$k_{78} = k_x \times e^{-Qn \times Em/53} \quad (27)$$

$$k_{87} = k_x \times F'2n_i \times e^{Qn \times Em/53} \quad (28)$$

$$k_{81} = k_x \times e^{-Qn \times Em/53} \quad (29)$$

$$k_{18} = k_x \times F'1n_i \times e^{Qn \times Em/53} \quad (30)$$

The solution was calculated with a generalized King-Altman procedure for cyclical, unbranched state diagrams. With E_1 to E_8 designated as the fractions of the exchanger in the respective states, the cycle rate, R_{net}, is

$$R_{net} = E_2 \times k_{21} - E_1 \times k_{12} \quad (31)$$

Unidirectional fluxes were calculated as described previously (Hilgemann, 1988) by expanding the state diagram to treat separately ions originating from the extracellular side and from the cytoplasmic side. Including the appropriate states for calculation of both unidirectional sodium and unidirectional calcium movements, the E8 model expands to a 20-state model. For brevity, the expanded state diagram and calculation routines are not presented.

The fitted parameters for the E8 model were as follows: Kc_o = 4.755 mM, $K1n_o$ = 32861 mM, $K2n_o$ = 106.5 mM, $K3n_o$ = 1.233 mM, Kc_i = 0.0233 mM, $K1n_i$ = 375.4 mM, $K2n_i$ = 3.917 mM, $K3n_i$ = 14.398 mM, Q_{ci} = 0.3322, and Q_{co} = −0.1644. For simplicity, $Kcn_i = K3n_i$. Q_n = 0.1387.

The E4 model. For the E4 model, the E_1 and E_2 states included fractions of the enzyme with occluded Ca. For simplicity, the occluded fractions of these states are assumed to be in 1:1 equilibrium with the fractions occupied by Ca but not occluded. For subsequent calculation of the rate constants, the Fc fractions are redefined as the fractions of the E_1 and E_2 states with occluded Ca ions.

$$D_o = \frac{C_o}{Kc_o} \times e^{Qco \times Em/26.5} + \frac{C_o}{Kc_o} + 1 + \frac{N_o}{K1n_o} + \frac{N_o^2}{K1n_o \times K2n_o} + \frac{N_o^3}{K1n_o \times K2n_o \times K3n_o} \quad (32)$$

$$Fc_o = \left(\frac{C_o}{Kc_o} \times e^{Qco \times Em/26.5}\right) \Big/ D_o \quad (33)$$

$$F3n_o = \left(\frac{N_o^3}{K1n_o \times K2n_o \times K3n_o}\right) \Big/ D_o \quad (34)$$

$$D_i = \frac{C_i}{Kc_i} \times e^{-Qco \times Em/26.5} + \frac{C_i}{Kc_i} + \frac{C_i \times N_i}{Kc_i \times Knc_i} + 1 + \frac{N_i}{K1n_i} + \frac{N_i^2}{K1n_i \times K2n_i} + \frac{N_i^3}{K1n_i \times K2n_i \times K3n_i} \quad (35)$$

$$Fc_i = \left(\frac{C_i}{Kc_i} \times e^{-Qci \times Em/26.5}\right) \Big/ D_i \tag{36}$$

$$F3n_i = \left(\frac{N_i^3}{K1n_i \times K2n_i \times K3n_i}\right) \Big/ D_i \tag{37}$$

Also, preliminary calculations are required of the fractions of E_1 and E_2 states whose first two Na binding sites are occupied by Na (F'_{2ni} and $F'2n_o$):

$$F'2n_i = \left(\frac{N_i^2}{K1n_i \times K2n_i} + \frac{N_i^3}{K1n_i \times K2n_i \times K3n_i}\right) \Big/ D_i \tag{38}$$

$$F'2n_o = \left(\frac{N_o^2}{K1n_o \times K2n_o} + \frac{N_o^3}{K1n_o \times K2n_o \times K3n_o}\right) \Big/ D_o \tag{39}$$

And finally, the fractions of E_3 and E_4 states whose third Na binding sites are occupied by Na ($F'3n_i$ and $F'3n_o$) are calculated:

$$F'3n_i = \left(\frac{N_i}{K3n_i}\right) \Big/ \left(1 + \frac{N_i}{K3n_i}\right) \tag{40}$$

$$F'3n_o = \left(\frac{N_o}{K3n_o}\right) \Big/ \left(1 + \frac{N_o}{K3n_o}\right) \tag{41}$$

For the calculations presented, Q_{co} was set to 0, and the voltage dependence in Na translocation was placed entirely on the reactions occluding two Na ions:

$$Q_{ci} + 2 \times Q_n = 1 \tag{42}$$

The rate constants are:

$$k_{43} = k_x \times F3n_i \tag{43}$$

$$k_{34} = k_x \times F3n_o \tag{44}$$

$$k_{32} = k_x \times e^{Em \times Qn/53} \tag{45}$$

$$k_{23} = k_x \times F2n_o \times e^{-Em \times Qn/53} \tag{46}$$

$$k_{21} = k_x \times Fc_o \tag{47}$$

$$k_{12} = k_x \times Fc_i \tag{48}$$

$$k_{14} = k_x \times F2n_i \times e^{Em \times Qn/53} \tag{49}$$

$$k_{41} = k_x \times e^{-Em \times Qn/53} \tag{50}$$

With the temporary variables, x_1–x_4 and d, the solution of the four-state model is:

$$x_1 = k_{34} \times k_{23} \times (k_{14} + k_{12}) + k_{21} \times k_{14} \times (k_{34} + k_{32}) \tag{51}$$

$$x_2 = k_{43} \times k_{14} \times (k_{23} + k_{21}) + k_{23} \times k_{12} \times (k_{43} + k_{41}) \tag{52}$$

$$x_3 = k_{43} \times k_{32} \times (k_{14} + k_{12}) + k_{41} \times k_{12} \times (k_{34} + k_{32}) \tag{53}$$

$$x_4 = k_{34} \times k_{41} \times (k_{23} + k_{21}) + k_{32} \times k_{21} \times (k_{43} + k_{41}) \tag{54}$$

$$d = x_1 + x_2 + x_3 + x_4 \tag{55}$$

$$E_1 = x_1/d \tag{56}$$

$$E_2 = x_2/d \tag{57}$$

$$E_3 = x_3/d \tag{58}$$

$$E_4 = x_4/d \tag{59}$$

$$R_{net} = E_2 \times k_{21} - E_1 \times k_{12} \tag{60}$$

Unidirectional fluxes were calculated as described for the E8 model. Again for the sake of brevity, solutions are not communicated.

The fitted parameters for the E4 model were as follows: Kc_o = 3.663 mM, $K1n_o$ = 1628 mM, $K2n_o$ = 561.4 mM, $K3n_o$ = 4.633 mM, Kc_i = 0.0207 mM, $K1n_i$ = 395.3 mM, $K2n_i$ = 2.289 mM, $K3n_i$ = 26.44 mM, Q_{ci} = 0.1369, and, for simplicity, Q_{co} = 0, and accordingly, Q_n = 0.4315.

The E2 model. For the E2 model, the E_1 and E_2 states include occlusion reactions for both Ca-loaded and the fully Na-loaded fractions. For simplicity, the occlusion reactions are simulated to be in 1:1 equilibrium with the ion-loaded fractions, and the dissociation constants of the second and third sodium binding reactions were equal. For the results presented, charge movement carried by each of the occlusion reactions was treated as a free parameter. Accordingly,

$$Q_{co} + Q_{ci} + Q_{no} + Q_{ni} = 1 \tag{61}$$

The reactions between states are assumed to be voltage independent, and a maximum rate constant for the calcium translocation reaction (K_{ca}) was fitted separately from the sodium translocation rate (K_{na} = 1,000 s^{-1}). Affinity of the extracellular Ca binding reaction and the first Na binding reaction were decreased equally from those on the cytoplasmic side by an asymmetry factor (F_{asym}). This conforms to one possible explanation for the lower apparent affinities on the extracellular side, namely, that the empty carrier on the extracellular side is in equilibrium with a state unavailable for ion binding. The dissociation constants for the second and third Na binding reactions are the same in the E_1 and E_2 states in the simulations presented. Calculation of the E2 model proceeds as follows, where $F3n_o$ and $F3n_i$ are now the state fractions with three occluded Na ions:

$$D_o = \frac{C_o}{Kc_o} \times e^{Qco \times Em/26.5} + \frac{C_o}{Kc_o} + 1 + \frac{N_o}{K1n_o} + \frac{N_o^2}{K1n_o \times K2n_o} + \frac{N_o^3}{K1n_o \times K2n_o \times K3n_o} + \frac{N_o^3}{K1n_o \times K2n_o \times K3n_o} \times e^{-Qno \times Em/26.5} \tag{62}$$

$$Fc_o = \left(\frac{C_o}{Kc_o} \times e^{Qco \times Em/26.5}\right) \Big/ D_o \tag{63}$$

$$F3n_o = \left(\frac{N_o^3}{(K1n_o \times K2n_o \times K3n_o)} \times e^{-Qno \times Em/26.5}\right) \Big/ D_o \tag{64}$$

$$D_i = \frac{C_i}{Kc_i} + \frac{C_i}{Kc_i} \times e^{-Qci \times Em/26.5} + \frac{C_i \times N_i}{Kc_i \times Knc_i} + 1 + \frac{N_i}{K1n_i} + \frac{N_i^2}{K1n_i \times K2n_i} + \frac{N_i^3}{K1n_i \times K2n_i \times K3n_i} + \frac{N_i^3}{K1n_i \times K2n_i \times K3n_i} \times e^{Qni \times Em/26.5} \tag{65}$$

$$Fc_i = \left(\frac{C_i}{Kc_i} \times e^{-Qci \times Em/26.5}\right) \Big/ D_i \tag{66}$$

$$F3n_i = \left(\frac{N_i^3}{K1n_i \times K2n_i \times K3n_i} \times e^{Qni \times Em/26.5}\right) \Big/ D_i \tag{67}$$

$$k_{12} = F3n_i \times k_{na} + Fc_i \times k_{ca} \tag{68}$$

$$k_{21} = F3n_o \times k_{na} + Fc_o \times k_{ca} \tag{69}$$

$$E_1 = k_{21}/(k_{12} + k_{21}) \tag{70}$$

$$E_2 = k_{12}/(k_{12} + k_{21}) \tag{71}$$

$$R_{net} = E_2 \times k_{21} - E_1 \times k_{12} \tag{72}$$

The fitted parameters for the E2 model were as follows: F_{asym} = 243.5, Kc_i = 0.0162 mM, $Kc_o = Kc_i \times F_{asym}$ mM, $K1n_i$ = 125.9 mM, $K1n_o = K1n_i \times F_{asym}$ mM. $K2n_i = K2n_o$ = 11.31 mM, $K3n_i = K3n_o$ = 11.31 mM, Q_{ci} = 0.254, Q_{ni} = 0.381, Q_{no} = 0.365, and for simplicity, Q_{co} = 0.0. With K_{na} = 1000 s^{-1}, K_{ca} = 1,744 s^{-1}.

Voltage-dependent Occlusion of Cytoplasmic Calcium

Fig. 20 shows the *I-V* relations of the E8 model with the parameter settings used to reconstruct data in Results (solid lines) and with the voltage dependence of Ca_i occlusion removed and partitioned evenly to the Na occlusion reactions (dashed curves). Fig. 20 *A* shows the *I-V* relations under the conditions of current reversal (2 mM Ca_o and 150 mM Na_o, 2 μM free Ca_i). The three *I-V* relations shown are with 100, 15, and 6 mM Na_i, from left to right. Without a voltage dependence of Ca_i occlusion, voltage dependence of the inward current is lost at low Ca_i concentrations. This is further illustrated in Fig. 20 *B* for the isolated inward current (0 mM Ca_o and 150 mM Na_o; 0 mM Na_i) with 0.8 μM, 3 μM, and 1 mM Ca_i. Note the saturation of the inward exchange current with hyperpolarization without voltage-dependent cytoplasmic Ca occlusion (dashed lines).

Voltage Dependence of Ion Self-exchange

Fig. 21 describes the voltage dependence of ion self-exchange in the E8 model. The characteristics to be described are qualitatively consistent with self-exchange experiments with the cardiac exchanger reconstituted in proteoliposomes (Khananshvili, 1991). Fig. 21 *A* shows the voltage dependence of calcium-calcium exchange in the absence of Na. Curve *1* is under saturating conditions (5 mM Ca_o and 0.1 mM Ca_i) and curve *2* is under nonsaturating conditions with respect to the cytoplasmic side (5 mM Ca_o and 3 μM Ca_i). Under nonsaturating conditions the calcium-calcium exchange decreases monotonically with depolarization, equivalent to results of DiPolo and Beaugé (1990). At low Ca_i concentrations, the voltage dependence of the calcium-calcium exchange becomes nearly identical to that of sodium-calcium exchange (not shown).

Fig. 21 *B* shows the voltage dependence of sodium-sodium exchange in the absence of calcium. Curve *1* is under nearly saturating conditions with 150 mM Na_o and 80 mM Na_i. Curve *2* is under nonsaturating conditions (50 mM Na_o and 80 mM Na_i). Note the relatively shallow voltage dependence under saturating conditions (curve *1*). Between 0 and −50 mV, the calculated sodium-sodium exchange decreases by ~15%. If asymmetries of the Na occlusion reactions are allowed, voltage dependence of the saturated sodium-sodium exchange can show

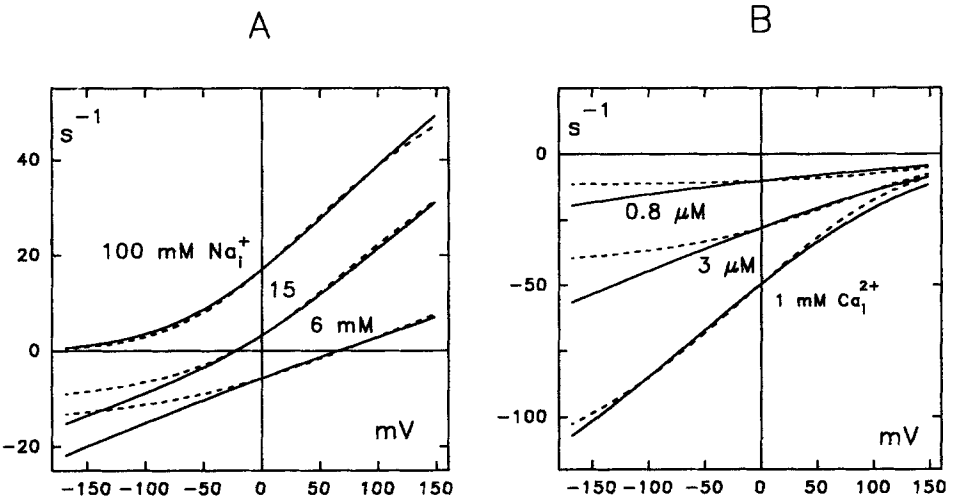

FIGURE 20. Effect on *I-V* relations of removing voltage dependence of Ca_i occlusion: E8 model. Solid curves are with parameters as described. Dashed curves are after removal of Ca_i voltage dependence and partitioning to the Na occlusion reactions. *A* is for conditions of current reversal (2 mM Ca_o and 150 mM Na_o; 2 μM Ca_i) at 100, 15, and 6 mM Na_i. *B* gives results for the isolated inward exchange current (0 mM Ca_o and 150 mM Na_o; 0 mM Na_i). The results are for 0.8 μM, 3 μM, and 1 mM Ca_i.

a monotonic decrease or increase with depolarization, and shallow U shapes are also possible (not shown). Experimentally, the largest possible effects of voltage on sodium-sodium exchange should be obtained by subtracting results with saturating Na concentrations from results with a subsaturating Na concentration on one side (i.e., equivalent to the difference between curves *1* and *2* of Fig. 21 *B*).

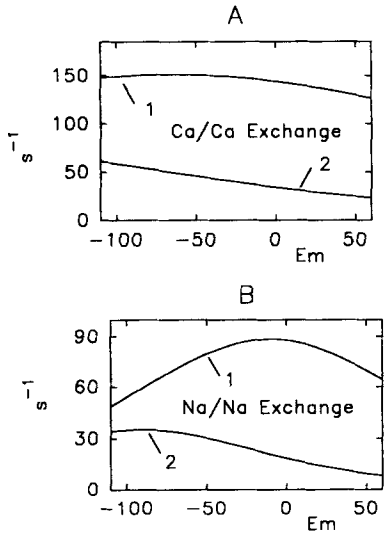

FIGURE 21. Characteristics of modeled ion self-exchange in the E8 model. *A* shows results for calcium-calcium exchange with 5 mM Ca_o and 0.1 mM Ca_i (curve *1*) and with 5 mM Ca_o and 3 μM Ca_i (curve *2*). *B* shows sodium-sodium exchange with 150 mM Na_o and 80 mM Na_i (curve *1*) and with 50 μM Na_o and 80 μM Na_i (curve *2*).

Outward Exchange Current in Intact Myocytes

Since we do not have detailed results on Ca_o and Na_o interactions, we describe here simulations of one data set from intact myocytes mentioned in the Discussion. Fig. 22 shows the *I-V* relations for outward exchange current at different Ca_o concentrations in the presence of 140 mM Na_o (Ehara et al., 1989). The results, presented as data points, are in the presence of 40 mM Na_i and 55 nM Ca_i. The solid curves in Fig. 22 give the *I-V* relations predicted by the E8 model with the parameters used for all data presented in Results. We point out that these data were not included in the data base used for fitting. The model describes the data in remarkable detail. Of particular note is the fact that the *I-V* relations do not lose voltage dependence as Ca_o concentration is reduced, as is the case in the absence of extracellular Na_o.

Limitations of Model-fitting Approach

Finally, we note limitations of the model-fitting approach that we encountered in the course of this work. The model formulations described in this Appendix were chosen for presentation because they utilize the smallest number of free parameters, in our experience, which allowed good reconstructions of the data base. With these formulations, the data fits presented are

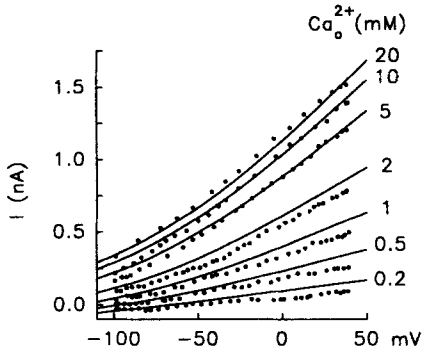

FIGURE 22. Predicted *I-V* relations for outward exchange current in the presence of 140 mM Na_o. The data points (*open circles*) were taken from the results of Ehara et al. (1989) with intact guinea pig myocytes (55 nM Ca_i, 40 mM Na_i). Solid curves are the predicted relationships of the E8 model with no parameter changes from those used in Results. See text for further explanations.

unique in that the fitting procedure converged to the same solutions of the individual models when it was initiated with widely different estimates of the model parameters. This was not the case when additional details or complexities were introduced into the models, such as asymmetries of the forward and backward rate constants, or the assignment of individual rate constants and voltage dependencies to each transition in the E4 and E8 models. When this was done, the quality of data fits increased only marginally, and multiple minima could usually be located by initiating the fitting procedure from different parameter estimates. Clearly, these findings drastically limit the consideration of more detailed models than those presented here until different types of experimental data become available (e.g., more detailed information on ion self-exchange and partial electrogenic reactions).

We thank Henry Liao for technical assistance. We thank Dr. Shmuel Muallem and Dr. Anthony Collins for helpful discussions and comments. D. Hilgemann acknowledges Dr. J. H. Mensing for many prescient discussions about the electrogenicity of cardiac sodium-calcium exchange (1977–1979).

This work was supported by NIH grant R29 HL-45240, an Established Investigatorship, and a Grant-in-Aid of the American Heart Association to D. W. Hilgemann, and by a grant from the Japan Heart Foundation to S. Matsuoka.

Original version received 29 July 1992 and accepted version received 25 September 1992.

REFERENCES

Allen, T. J. A., and P. F. Baker. 1986*a*. Comparison of the effect of potassium and membrane potential on the calcium-dependent sodium efflux in squid axons. *Journal of Physiology*. 378:53–76.

Allen, T. J. A., and P. F. Baker. 1986*b*. Influence of membrane potential on calcium efflux from giant axons of *Loligo*. *Journal of Physiology*. 378:77–96.

Blaustein, M. P., and J. M. Russell. 1975. Sodium-calcium exchange and calcium-calcium exchange in internally dialyzed squid giant axons. *Journal of Membrane Biology*. 22:285–312.

Bridge, J. H. B., J. Smolley, K. W. Spitzer, and T. K. Chin. 1991. Voltage dependence of sodium-calcium exchange and the control of calcium extrusion in the heart. *Annals of the New York Academy of Sciences*. 639:34–47.

Collins, A., A. V. Somlyo, and D. W. Hilgemann. 1992. The giant cardiac membrane patch method: stimulation of outward Na^+-Ca^{2+} exchange current by MgATP. *Journal of Physiology*. 454:27–57.

DiPolo, R., and L. Beaugé. 1990. Asymmetrical properties of the Na-Ca exchange in voltage-clamped, internally dialyzed squid axons under symmetrical ionic conditions. *Journal of General Physiology*. 95:819–835.

DiPolo, R., F. Bezanilla, C. Caputo, and H. Rojas. 1985. Voltage dependence of the sodium-calcium exchange in voltage-clamped, dialyzed squid axons. *Journal of General Physiology*. 86:457–478.

Earm, Y. E., W. K. Ho, and I. S. So. 1990. Inward current generated by sodium-calcium exchange during the action potential in single atrial cells of the rabbit. *Proceedings of the Royal Society of London*. B240:61–81.

Ehara, T., S. Matsuoka, and A. Noma. 1989. Measurement of reversal potential of Na^+-Ca^{2+} exchange current in single guinea-pig ventricular cells. *Journal of Physiology*. 410:227–249.

Gadsby, D. C., M. Noda, R. N. Shepherd, and M. Nakao. 1991. Influence of external monovalent cations on Na-Ca exchange current-voltage relationships in cardiac myocytes. *Annals of the New York Academy of Sciences*. 639:140–146.

Greenspan, D. 1974. Discrete Numerical Methods in Physics and Engineering. Academic Press, New York. 12–22.

Hilgemann, D. W. 1988. Numerical approximation of sodium-calcium exchange. *Progress in Biophysics and Molecular Biology*. 51:1–45.

Hilgemann, D. W. 1990. Regulation and deregulation of cardiac Na^+-Ca^{2+} exchange in giant excised sarcolemmal membrane patches. *Nature*. 344:242–245.

Hilgemann, D. W., and A. Collins. 1992. Mechanism of cardiac Na^+-Ca^{2+} exchange current stimulation by MgATP: possible involvement of aminophospholipid translocase. *Journal of Physiology*. 454:59–82.

Hilgemann, D. W., A. Collins, D. P. Cash, and G. A. Nagel. 1991*a*. Cardiac Na^+-Ca^{2+} exchange system in giant membrane patches. *Annals of the New York Academy of Sciences*. 639:126–139.

Hilgemann, D. W., A. Collins, and S. Matsuoka. 1992*a*. Steady-state and dynamic properties of cardiac sodium-calcium exchange. Secondary modulation by cytoplasmic calcium and ATP. *Journal of General Physiology*. 100:933–961.

Hilgemann, D. W., S. Matsuoka, G. A. Nagel, and A. Collins. 1992*b*. Steady-state and dynamic properties of cardiac sodium-calcium exchange. Sodium-dependent inactivation. *Journal of General Physiology*. 100:905–932.

Hilgemann, D. W., D. A. Nicoll, and K. D. Philipson. 1991*b*. Charge movement during Na^+ translocation by native and cloned cardiac Na^+/Ca^{2+} exchanger. *Nature*. 352:715-718.

Hilgemann, D. W., K. D. Philipson, and D. A. Nicoll. 1992*c*. Possible charge movement of extracellular Na^+ binding by Na/K pump and cardiac Na/Ca exchanger in giant patches. *Biophysical Journal*. 61:A390. (Abstr.)

Hille, B. 1992. Ionic Channels of Excitable Membranes. 2nd ed. Sinauer Associates, Inc., Sunderland, MA. 607 pp.

Horackova, M., and G. Vassort, 1979. Sodium-calcium exchange in regulation of cardiac contractility. *Journal of General Physiology.* 73:403–424.

Jennings, M. L., R. K. Schulz, and M. Allen. 1990. Effects of membrane potential on electrically silent transport: potential-independent translocation and asymmetric potential-dependent substrate binding to the red blood cell anion exchange protein. *Journal of General Physiology.* 96:991–1012.

Khananshvili, D. 1990. Distinction between the two basic mechanisms of cation transport in the cardiac Na^+-Ca^{2+} exchange system. *Biochemistry.* 29:2437–2442.

Khananshvili, D. 1991. Voltage-dependent modulation of ion binding and translocation in the cardiac Na^+-Ca^{2+} exchange system. *Journal of Biological Chemistry.* 266:13764–13769.

Kimura, J., S. Miyamae, and A. Noma. 1987. Identification of sodium-calcium exchange current in single ventricular cells of guinea-pig. *Journal of Physiology.* 384:199–222.

Lagnado, L., L. Cervetto, and P. A. McNaughton. 1988. Ion transport by the Na-Ca exchange in isolated rod outer segments. *Proceedings of the National Academy of Sciences, USA.* 85:4548–4552.

Läuger, P. 1987. In memoriam Peter F. Baker: Voltage dependence of sodium-calcium exchange: predictions from kinetic models. *Journal of Membrane Biology.* 99:1–11.

Läuger, P. 1991. Electrogenic Ion Pumps. Sinauer Associates, Inc., Sunderland, MA. 313 pp.

Li, J., and J. Kimura. 1990. Translocation mechanism of Na-Ca exchange in single cardiac cells of guinea pig. *Journal of General Physiology.* 96:777–788.

Li, J., and J. Kimura. 1991. Translocation mechanism of cardiac Na-Ca exchange. *Annals of the New York Academy of Sciences.* 639:48–60.

McNaughton, P. A. 1991. Fundamental properties of the Na-Ca exchange: an overview. *Annals of the New York Academy of Sciences.* 639:2–9.

Miura, Y., and J. Kimura. 1989. Sodium-calcium exchange current: dependence on internal Ca and Na and competitive binding of external Na and Ca. *Journal of General Physiology.* 93:1129–1145.

Mullins, L. J. 1979. The generation of electric currents in cardiac fibers by Na/Ca exchange. *American Journal of Physiology.* 236:C103–C110.

Niggli, E., and W. J. Lederer. 1991. Molecular operations of the sodium-calcium exchanger revealed by conformation currents. *Nature.* 349:621–624.

Reeves, J. P., and K. D. Philipson. 1989. Sodium-calcium exchange activity in plasma membrane vesicles. *In* Sodium-Calcium Exchange. T. J. A. Allen, D. Noble, and H. Reuter, editors. Oxford University Press, New York. 27–53.

Reeves, J. P., and J. L. Sutko. 1983. Competitive interactions of sodium and calcium with the sodium-calcium exchange system of cardiac sarcolemmal vesicles. *Journal of Biological Chemistry.* 258:3178–3182.

Tanford, C. 1982. Simple model for the chemical potential change of a transported ion in active transport. *Proceedings of the National Academy of Sciences, USA.* 79:2882–2884.